Title
BETA SPECTRA OF TILE MIRROR NUCLEI WITH A = 19 TO 39

Author
Welch, Jasper A.

Publication Date
1957-08-02

UCRL 3888

UNIVERSITY OF CALIFORNIA

Radiation Laboratory

BERKELEY, CALIFORNIA

DISCLAIMER

UCRL-3888

UNIVERSITY OF CALIFORNIA

Radiation Laboratory
Berkeley, California

Contract No. W-7405-eng-48

BETA SPECTRA OF THE MIRROR NUCLEI WITH A=19 TO 39

Jasper A. Welch, Jr.

(Thesis)

August 2, 1957

Printed for the U. S. Atomic Energy Commission

BETA SPECTRA OF THE MIRROR NUCLEI WITH A = 19 to 39

Contents

BETA SPECTRA OF THE MIRROR NUCLEI WITH A=19 TO 39

Jasper A. Welch, Jr.

Radiation Laboratory
University of California
Berkeley, California

August 2, 1957

ABSTRACT

The positron spectra and half lives of all the mirror nuclei ($Z = \frac{A \pm 1}{2}$) with $19 \leqslant A \leqslant 39$ have been systematically measured with a 180° deflection uniform-magnetic-field spectrometer. The ground-state transition energies were used to compute Coulomb energy differences between mirror pairs.

Deviations of these Coulomb energy differences from a smooth variation with A are explained in great detail by a nuclear shell model using an isotropic harmonic oscillator potential well. The data definitely support a symmetry for the proton wave functions characteristic of jj coupling in the state of lowest seniority, with magic number effects at Z = 14 and 16 as well as Z = 8 and 20.

Comparison of the ft values obtained with experimental nuclear magnetic moments gives the following values for the partial coupling constants for the Fermi and Gamow-Teller β interactions:

$$g_F^2 = \frac{1}{6700} \text{ sec}^{-1},$$

$$g_{GT}^2 = \frac{1}{4800} \text{ sec}^{-1}.$$

I. INTRODUCTION

A. The Role of Nuclear Coulomb Energy

The total binding-energy difference between isobars is composed of contributions from nuclear forces, repulsive Coulomb forces between protons, and the neutron-proton mass difference. The nuclear Coulomb energy depends upon the spatial correlations of the several protons in the nucleus, and its value is indicative not only of the general size of nuclei but also of the spatial symmetry of the proton wave functions.[1,2]

In the nuclear shell model with charge-independent nuclear forces, the specific nuclear contribution to the binding energy is the same for pairs of isobars characterized by

$$Z = \frac{A \pm 1}{2}, \quad Z = \frac{A \pm 2}{2}, \quad \text{etc.}^{3}$$

Thus in these cases we may obtain the Coulomb energy difference by simply correcting the total binding-energy difference for the neutron-proton mass ratio. Experimental total binding-energy differences are obtained from reaction energy and beta-disintegration energy measurements. In very light nuclei the perturbation of the Coulomb forces somewhat disturbs this nuclear equivalence.

B. Experimental Situation

The nuclear species $Z = \frac{A \pm 1}{2}$ are called mirror nuclei and have been the objects of considerable theoretical[1,4-12] and experimental[13-18] attention. We shall label mirror pairs by their mass number, A_{mp}. Very accurate experimental binding-energy data are available for $A_{mp} \leqslant 21$ from reaction-energy measurements.[19] This experiment has obtained, from positron-decay disintegration energies, a systematic, accurate set of binding-energy differences throughout the region $19 \leqslant A \leqslant 39$. The earlier experimental situation was characterized by much disagreement,[17] although several experiments of high precision have been performed recently.[15,16]

The species $Z = \frac{A \pm 2}{2}$ together with the self-mirrored species $Z = A/2$ are called triads. We shall label the triads with their mass number, A_t. Investigations of positions of energy levels, and the shifts of them caused by the Coulomb perturbation, have been made for $A_t \leq 14$.[2]

For higher A_t the masses of the neutron-rich members are known with fair precision, while for the proton-rich members some are known to a few hundred kilovolts[20] and others have not been identified. A study of the available data to check charge independence of nuclear forces has been made by Wilkinson[21] and reviewed in Section IV-E. This check indicates that the n-p bond may be slightly stronger than the n-n bond (1.5% ± 2.5%). Studies of the singlet scattering data imply the n-p bond may be slightly stronger (~3%) than the p-p bond.

Thus, our assumption of nuclear force equivalence of the ground states of the mirror nuclei seems fairly accurate.

C. Nuclear Radii

Besides Coulomb energy differences in mirror nuclei, there are several methods for making measurements of nuclear charge distributions and sizes:

1. Charge-sensitive methods:
   a. electron scattering
   b. μ-mesonic atoms and μ-meson scattering
   c. fine structure in x-ray spectra
   d. isotope shifts
   e. hyperfine structure in hydrogen
2. Range-of-nuclear-force methods:
   f. neutron-scattering experiments at a variety of energies
   g. proton and alpha-particle scattering
3. Combinations of 1 and 2:
   h. Weisacker semi-empirical mass formula
   i. alpha-particle radioactivities.

Detailed intercomparison of the theory and results of the various methods has been recently made by Ford and Hill[22], Hofstadter[23],

and Scott.[24]

Because nuclear Coulomb energies depend not only upon the "size" of the nucleus but also upon the overlap of the proton wave functions, nuclear radii deduced from data on mirror nuclei are highly dependent on the model used. Details of this dependence are discussed in Sections IV-A through IV-D.

Comparisons of radii from this experiment with those from high-energy electron scattering and μ-mesonic atoms are in Section IV-D.

D. Nuclear Matrix Elements

By measuring the lifetimes as well as the disintegration energies for all transitions, we obtained their comparative lifetimes, or ft values.[25] These values are compared with theoretical matrix elements and matrix elements based on measured magnetic moments of the daughter isobars[26,27] in Section IV-E. The latter comparison gives values for both the Fermi and Gamow-Teller β-decay interaction constants.

E. The Experiment

The radioisotopes were produced by deuteron and proton bombardments with the external beam of the 60-inch cyclotron at Crocker Laboratory, and by proton bombardments at the 32-Mev proton linear accelerator, as well as deuteron bombardments with the linac's Van de Graaff injector.

The beta spectra were measured with a 180°-deflection single-focusing magnetic spectrometer.

II. EXPERIMENTAL DESIGN AND PROCEDURE

A. Equipment

The beta spectra were measured with a uniform-field 180°-deflection single-focusing spectrometer (shown in Fig. 1). Although more elaborate designs have advantages of higher transmission and thus higher resolution for a given source strength,[28] we felt that it was more important for this experiment to use a simple design whose characteristics were well understood and whose calibration depends only on measurements of a length and a uniform magnetic field. The design was carried out along the lines suggested by Persico, et al.[29, 30] who developed formulae for maximizing transmission for a given resolution. The size of the orbit was, in fact, dictated by available power supplies, iron, and copper. The magnetic field was carefully mapped and calibrated to 0.1% against magnet current with commercial nuclear magnetic resonance equipment (Laboratory for Electronics probe and oscillator and Hewlett-Packard frequency counter checked against station WWV). The field along the central ray exhibited some droop near the ends of the orbit, as shown in Fig. 2. By plotting orbits, we found that this disturbance could be adequately taken into account by using the average magnetic field around the orbit. No other deviations greater than 0.1% were observed in the field uniformity.

Some characteristics of the spectrometer are given in Table I.

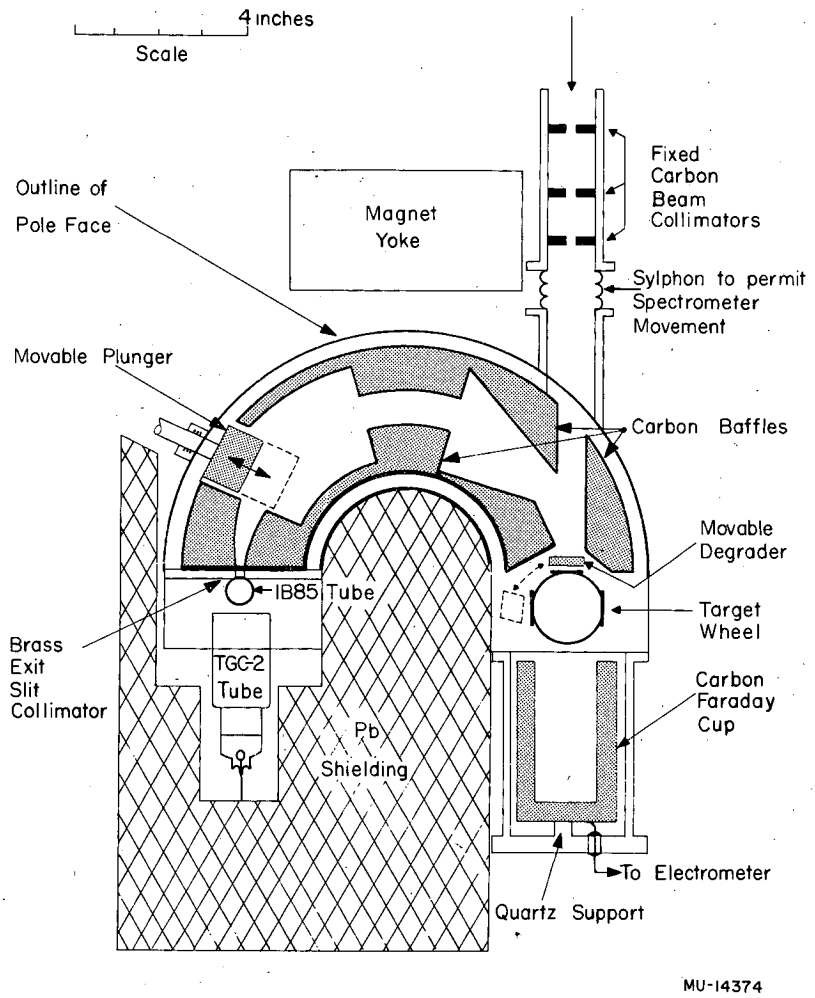

Fig. 1. Detail of spectrometer. A schematic cross section through the spectrometer perpendicular to the magnetic field is shown. Although several construction details are suppressed for clarity, the major components are drawn to scale and labeled.

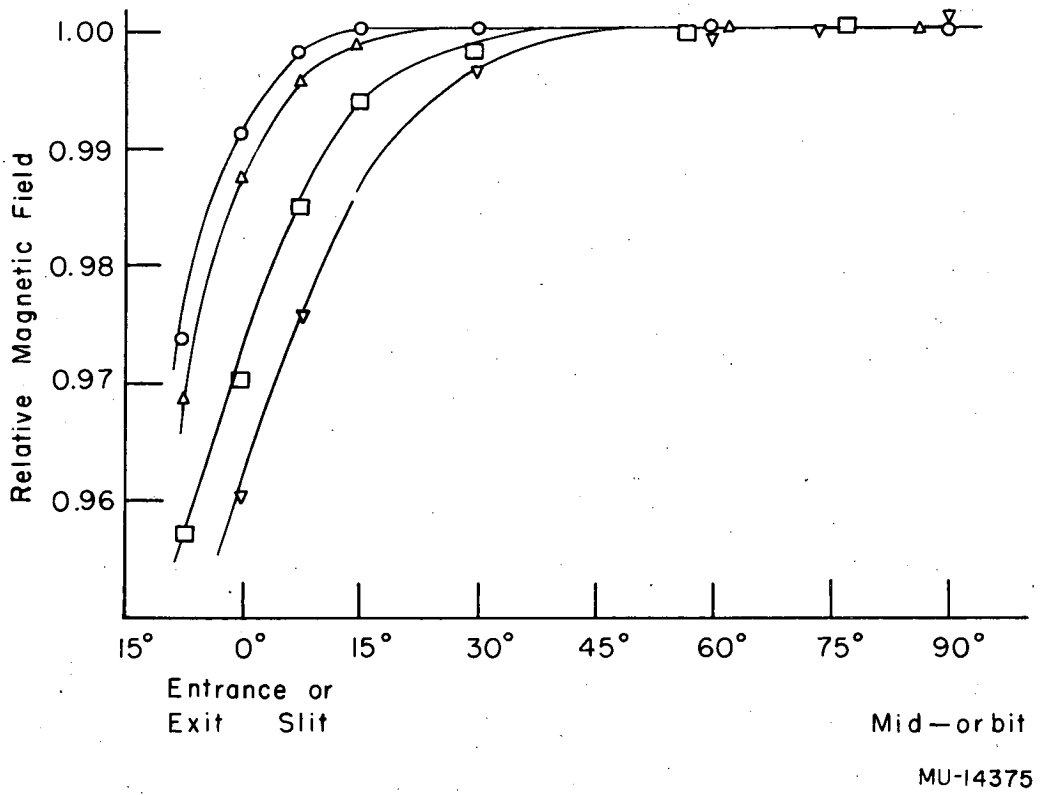

Fig. 2. Magnetic field along the central ray. The relative magnetic field, normalized to the mid-orbit value, is shown as a function of θ, the angular position around the orbit, for several field strengths. The field was symmetric about the mid-point and data from both sides are included. It proved sufficient to use the average magnetic field along the central ray to correct for this nonuniformity.

Table I

Beta-spectrometer characteristics

Energy range	0.5 to 6 Mev
Radius of orbit	10.20 cm
Maximum field	2200 gauss
Power required at maximum field	15 volts 100 amperes
Transmission (percentage 4π)	0.2%

Instrument settings	Required resolution (full width at half height)	
	1%	2.5%*
Entrance slit width	0.25 cm	0.30 cm
Exit slit width	0.25 cm	0.62 cm
Mid-orbit baffle (full width)	3.0 cm	3.5 cm
Height of orbit	3.75 cm	3.75 cm

*as used in this experiment

It should be pointed out that the transmission is the percentage of particles of a given momentum that are collected; increasing the exit slit width increases the counts received, as one then collects particles over a larger momentum interval.

We chose the 2.5% resolution because we needed the counting rate, and we found that it did not affect the Kurie-plot extrapolation (see Sec. III-C).

B. Physical Arrangement

Because of the short half lives encountered, the spectrometer was positioned so that the accelerator's external beam struck a target placed at the entrance of the orbit (Figs. 1, 3, and 4). To reduce background, everything that would be exposed to direct or scattered beam was fashioned of carbon, as the activities that could be produced therein are either very short-lived (12-millisecond N^{12}) or long-lived and emitting lower-energy positrons than those being studied. In either case discrimination was easy. The width of the source was determined by beam collimation. Compensation for the deflection of the beam by the spectrometer field was made with a lead-screw traverse for the whole magnet assembly. The bombarding particle's energy was controlled by a carbon degrader interposed just ahead of the target to reduce the beam spread due to multiple scattering in the degrader (Fig. 1). The degrader could be moved by a shaft through a vacuum seal powered by a "gadget" based on two Leedex stepping-switch solenoids.

C. Experimental Details

All target materials except aluminum were available in powder form. Targets were prepared by mixing the powder into a dope of styrofoam dissolved in benzene and then pouring the mixture onto a saran-wrap-covered surface. After the benzene evaporated, the saran wrap was peeled off and a tough, beam-resistant material remained which could be easily cut and sanded to the desired shape (0.25 by 1.5 in.) and thickness (80 mg/cm^2). Several targets were mounted on a wheel, and target selection could be made manually by a shaft through a vacuum seal.

The beam current was collected in a carbon Faraday cup just behind the target. The angular aperture was large, and no difference in beam collection was observed as the thickest degrader was moved in and out. Secondary electron emission from the cup was suppressed by the deepness of the cup and the fringing field of the spectrometer. The beam current was fed into an RC circuit (see Fig. 5) whose decay

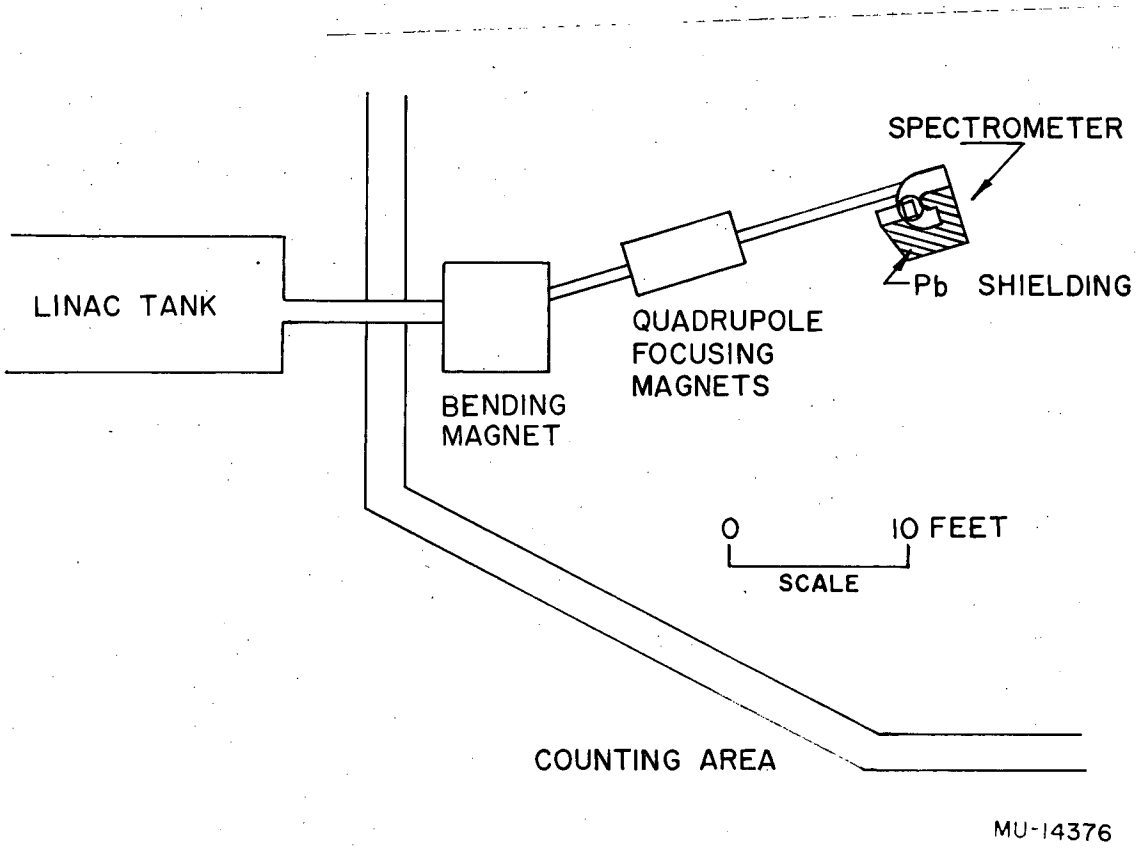

Fig. 3. Over-all arrangement for bombardments with the linear accelerator and the linac's van de Graaff injector.

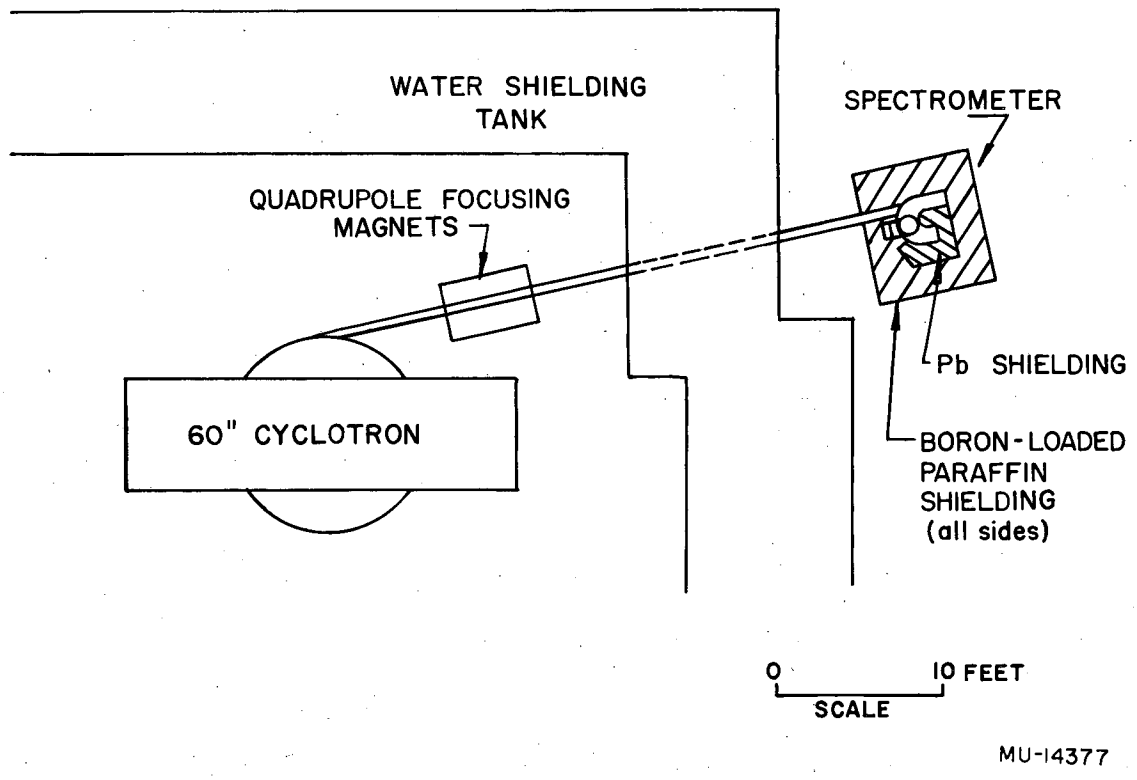

Fig. 4. Over-all arrangement for bombardments with the 60-inch cyclotron. Note the liberal use of neutron shielding.

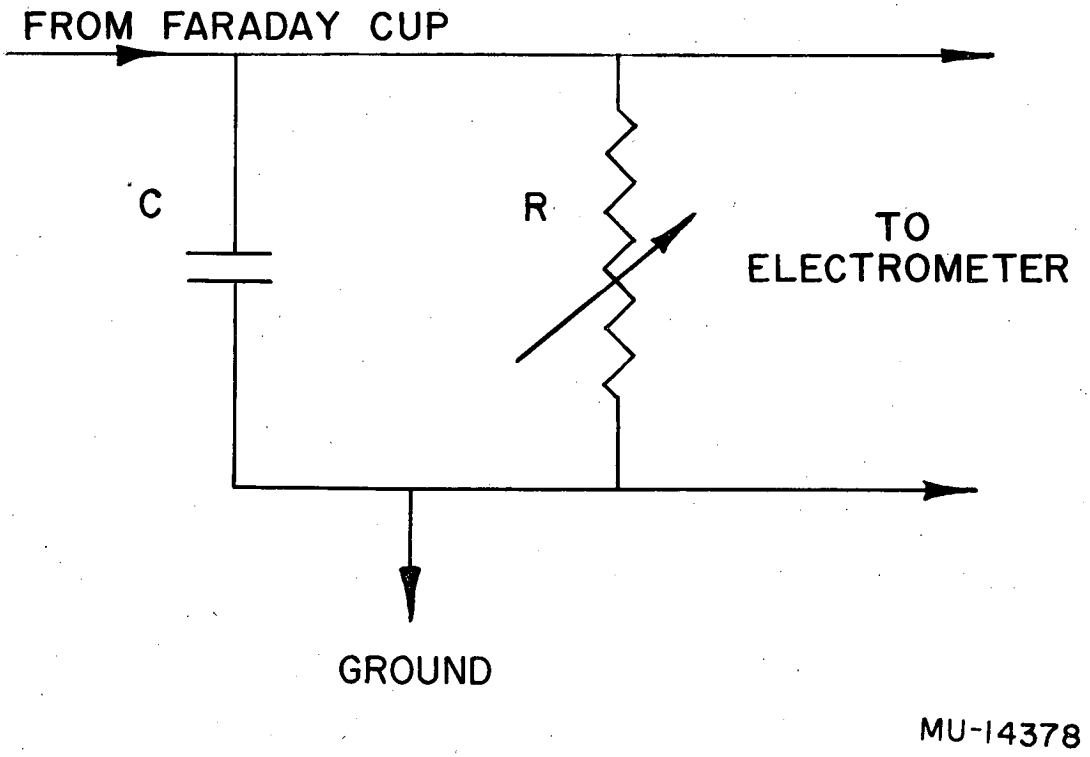

Fig. 5. Panofsky's circuit for monitoring the level of a short-lived activity produced by a time-varying accelerator current. R x C is set equal to the mean lifetime.

constant equaled that of the activity being investigated. This innovation by Professor W. K. H. Panofsky produces a voltage across the condenser at all times proportional to the activity of the target.

The beta particles were detected by two thin-walled gas proportional tubes in coincidence (Fig. 1). Many unsuccessful attempts were made to build a detector using a plastic scintillator and phototubes. There were two major difficulties: (a) because they scattered out of the scintillator in a random fashion, the almost monoenergetic positrons coming out of the spectrometer failed to give a well-defined pulse-height peak; (b) the plastic scintillators are quite sensitive to γ-ray background. Attempts to use a coincidence telescope helped some, but at great expense of positron-detection efficiency. The gas-tube telescope used is moderately energy-independent above 2 Mev (see Fig. 6), detects about 50% of all positrons that emerge from the spectrometer, and is at most 1/50 as sensitive to radium γ rays as the best scintillator arrangement we devised.

D. Electronics

We found that the gas proportional tubes required a 4-microsecond coincidence resolution in order to catch more than 99% of the possible coincidences. Therefore we used standard Radiation Laboratory slow electronics throughout.

A block diagram of the counting circuitry is given in Fig. 7, together with all auxiliary circuits for the experiment.

E. Experimental Procedure

With the degrader in position the beam was turned on and the target bombarded for three half lives. At this time the beam was abruptly shut off (at the linac with a mechanical gate after the injector; at the 60-inch cyclotron by switching the magnet off resonance), and simultaneously the movable degrader was flipped out of the β-particle orbit. The counts were recorded as a function of time after cessation of bombardment with a mechanical tandem-gate apparatus. The first few gates were set at half a half life, and succeeding ones set longer

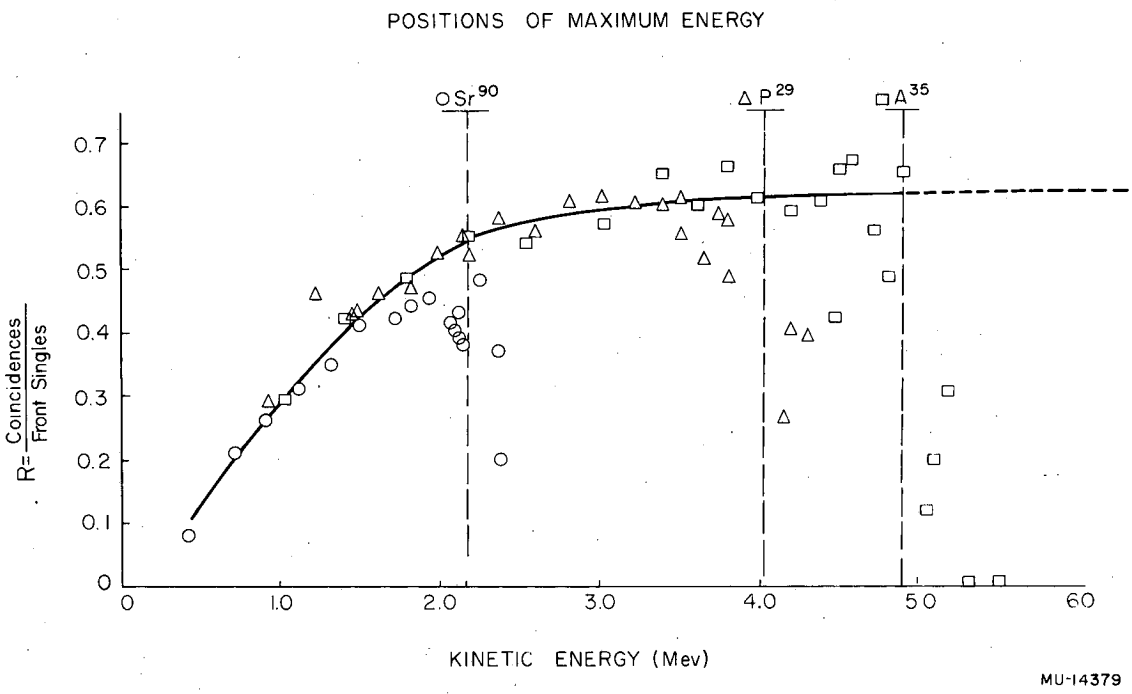

Fig. 6. Detection efficiency versus spectrometer energy setting. The end points of the several isotopes used are shown by vertical dashed lines. Note that the experimental points above each corresponding end point have efficiencies characteristic of much lower energies.

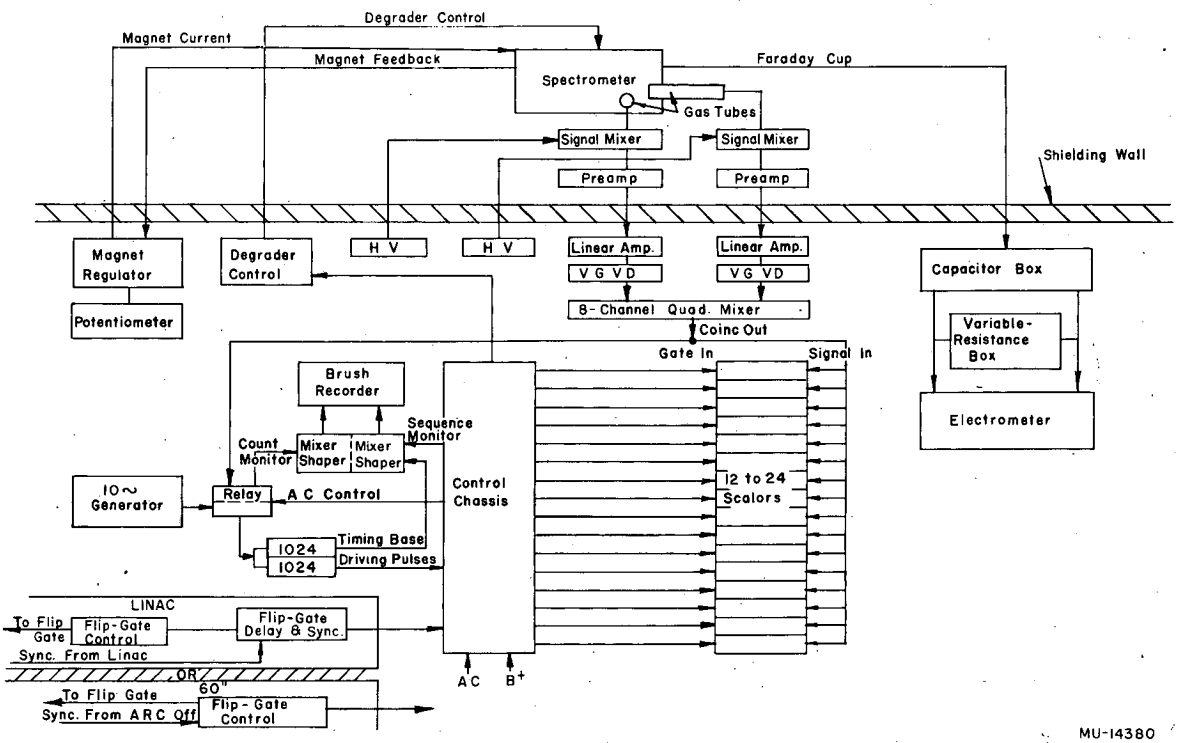

Fig. 7. Block diagram of the electronics used in this experiment. Note the alternate beam-control circuits for the two accelerators shown in the lower left-hand corner.

and longer to encompass a total recording time of about twelve half lives. This bombarding and counting routine was repeated enough times at each spectrometer energy to gather necessary counting statistics. Such a group of bombardments will be called a "run". As we got into the experiment, we found that it was necessary to carry through the routine on a very regular basis in order to maintain good knowledge of the background. In particular, the beam current should be uniform, the bombardment time should be uniform, the number of bombardments in each run should be constant, and the spacing between runs and between bombardments should be constant.

After every five target runs, described above, several of the following additional types of runs were made to ascertain the nature and amount of background:

(a) "Long." The time base and bombardment time were quadrupled and the number of bombardments was divided by four, to enhance the long-lived background, so as to more easily determine its decay rate and amount.

(b) "Short." The time base and bombardment time were divided by four and the number of bombardments was quadrupled, to enhance the short-lived background, so as to more easily determine its decay rate and amount.

(c) "Clear." Runs with any of the three aforementioned time bases could be made with an empty target holder (polystyrene without target material) in place to test the origin of any activity.

(d) "Plunger-in." There is built into the spectrometer a carbon plunger that can be inserted into the orbit 30° ahead of the exit slit. This prevents all positrons from reaching the detector, and hence allows direct measurement of all "nonorbit" counts. Runs could be made with plunger in for target, or clear, with any time base.

In the beginning this great flexibility was all but bewildering; it turned out that the important background sources were nonorbit or long-half-life activities formed in the target base. The manner of utilizing the background data is discussed in Section III-B.

III. THE DATA

The discussion in Sections III-A through III-C presents analysis methods peculiar to this experiment. The general methods of spectrum analysis are well documented in Siegbahn.[28] Kurie plots of the spectra and a tabulation of numerical results are given in Section III-C. Section III-D discusses the values of ft which were obtained. Sections III-E and III-F present an analysis of error for this experiment and some comparisons with other data.

A. Identification

Unique identification could always be made of the isotope responsible for the observed activity by proper choice of target material, bombarding particle, and particle energy, because approximate values for half life and end-point energy could be obtained from both theory[12] and experiment.[17] A summary of these choices is presented in Table II.

B. Background Correction and Half-Life Determination

The total count C(t, E) received for a regular target-in run is a function of time and spectrometer energy setting and consists of three components:

N(t, E), the desired target activity, a function of time and energy;

L(t, E), the positron activity induced in the target holder, plastic target base, and "extraneous" elements of the target compound;

B(t), the background reaching the detector not through the orbit, a function of time only.

The quantity B(t) is measured directly by the runs with plunger in, as described in Section II-D. This background arises from activities induced by the neutrons associated with the beam, and the annihilation radiation from positron activities formed by the beam in the collimators, target assembly, target, and Faraday cup. Careful regularization of the bombardment routine stabilized this quantity so that averages

Table II

Bombardment Schemes

Beta transition	Target[a]	Reaction	Bombarding particle energy (Mev)
$Ne^{19} \rightarrow F^{19}$	Li F	p, n	10
$Na^{21} \rightarrow Ne^{21}$	$Mg^{24}O$	p, α	10
$Mg^{23} \rightarrow Na^{23}$	Na_2CO_3	p, n	10
$Al^{25} \rightarrow Mg^{25}$	$Mg^{25}O$	p, n	10
$Si^{27} \rightarrow Al^{27}$	Al	p, n	10
$P^{29} \rightarrow Si^{29}$	Si	d, n	4
$S^{31} \rightarrow P^{31}$	P	p, n	10
$Cl^{33} \rightarrow S^{33}$	S	d, n	5
$A^{35} \rightarrow Cl^{35}$	NH_4Cl	p, n	10
$K^{37} \rightarrow A^{37}$	CaO	p, α	10
$Ca^{39} \rightarrow K^{39}$	K_2CO_3	p, n	10

[a]All targets contained C, H, and O as binding agents; isotopically enriched targets are shown by the enriched mass number used as a superscript.

could be taken over consecutive runs associated with one target material.

For the proton runs the quantity L(t, E) arose principally from among these reactions:

Reaction	Energy of β^+ (Mev)	Half life (min)
$C^{12}(p, pn)C^{11}$	0.96	20.5
$N^{14}(p, pn)N^{13}$	1.20	10.0
$N^{14}(p, n)O^{14}$	1.83	1.2
$O^{16}(p, pn)O^{15}$	1.7	2.1

Possible interference from $C^{12}(p, n)N^{12}$ (16.6-Mev β^+, 0.012 sec) was eliminated by delaying the start of counting 0.1 second after beam cessation. Thus L(t, E) should vanish above 2 Mev and should have no time components shorter than 1 minute; both these predictions were borne out during the experiment. For the deuteron runs some of the same activities were formed and, in addition, the reactions $S^{32}(d, \alpha)P^{30}$ (3.3-Mev β^+, 2.5 min) and $Si^{29}(d, n)P^{30}$ were observed. The decay rate of L(t, E) was measured by taking runs with a long time base.

The background subtraction proceeded as follows: first, the non-orbit background was subtracted from all runs and the difference,

$$C(t, E) - B(t) = N(t, E) + L(t, E),$$

was plotted on a logarithmic scale against time. If this plot deviated from the constant, known half life of N(t, E), a correction for L was applied. Through the last few points (timewise) a straight line with the previously determined slope of L was drawn and extrapolated to zero time. Values of L read from this line were then subtracted out to leave just N(t, E), which was again checked for proper half life. For most isotopes the time-zero value of N was larger than L plus B to within 3% of the end point.

The half life was determined from the combined data from several runs with high signal-to-background ratio.

C. Spectrum Analysis

In principle one could determine the relative spectral intensity at each energy by fitting the values of N(t) to an exponential decay and extrapolating the counting rate to time zero. But, having assured ourselves that only one half life was present, we found it more convenient and less subjective to use the total number of counts in the first four gates -- approximately two half lives. The runs were normalized for beam fluctuations by dividing the total counts by the sum of the capacitor voltages at the end of each bombardment, and reduced to a momentum spectrum by dividing through by the magnetic field.

A further correction was made for variation of detection efficiency with energy. This variation comes about because some positrons are scattered out of the rear proportional counter by the exit foil of the spectrometer (~15 mg/cm^2) and the walls of the front counter (~30 mg/cm^2). The scattering angle is a function of energy:[31]

$$\overline{\theta}^2 = \frac{(0.0013)\, D\,(\mathrm{mg/cm^2})}{E^2(\mathrm{Mev})}\,, \text{ for aluminum,}$$

and is equal to the acceptance angle of the rear counter at 1.5 Mev. The exact dependence of efficiency on energy was determined experimentally by taking the ratio

$$\text{Efficiency} = \frac{\text{plunger out - plunger in (for coincidences)}}{\text{plunger out - plunger in (for front singles)}}$$

as a function of energy for several isotopes.

The end-point energies of the spectra were determined by the usual Fermi-Kurie function analysis for allowed spectra, except that, for our low values of Z, the Coulomb-repulsion correction factor changed by at most 2% in the range 1 to 6 Mev and was omitted from the Kurie function.[32] The spectra are plotted in Figs. 8 through 18.

When the Kurie functions were first plotted, we found two types of deviations from straight lines:

First, the low-energy points bent upward, indicating the presence of branching transitions to excited levels of the daughter; the energy

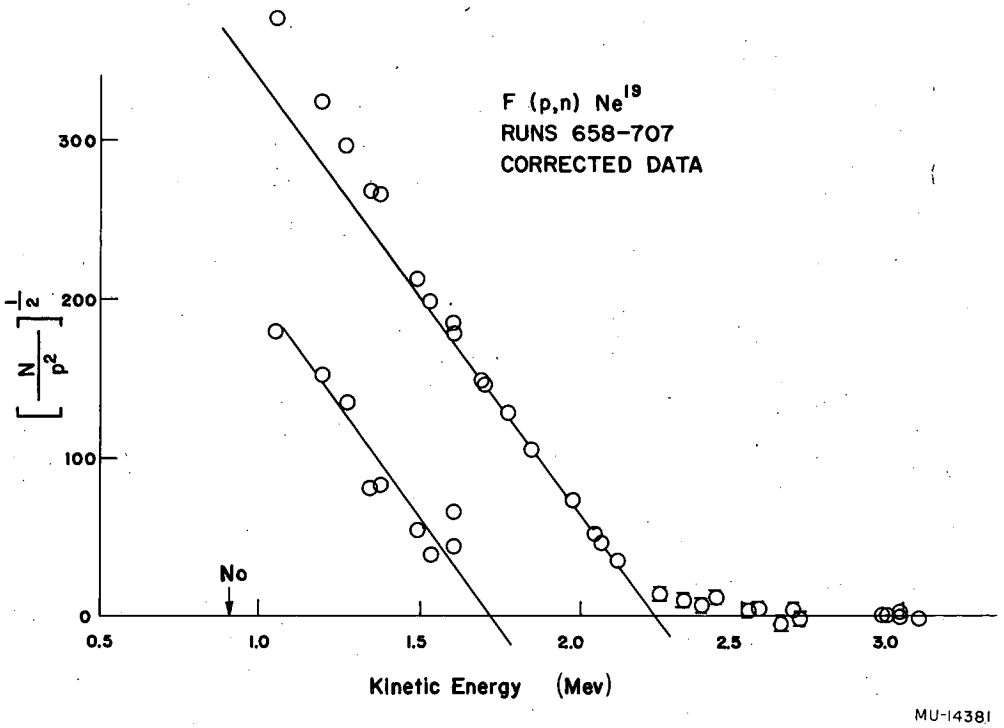

Fig. 8. Kurie plot for the isotope Ne^{19}. The experimental decomposition into branching transitions is shown. The arrows indicate positions of possible branching transitions deduced from known excited energy levels of the daughter isobars (see Table III). These arrows were entered after the components were resolved. (The foregoing remarks also apply to Figs. 9 through 18.)

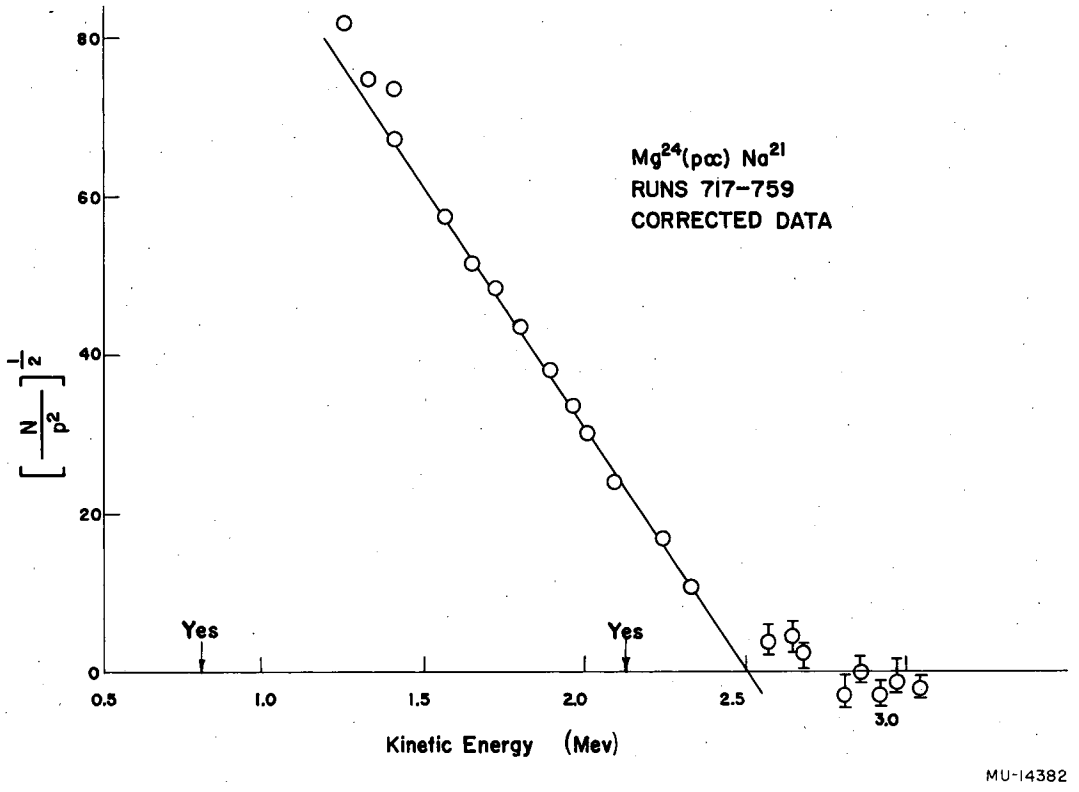

Fig. 9. Kurie plot for the isotope Na^{21}. Note the absence of branching transitions, in agreement with the findings by Schrank and Richardson.[33]

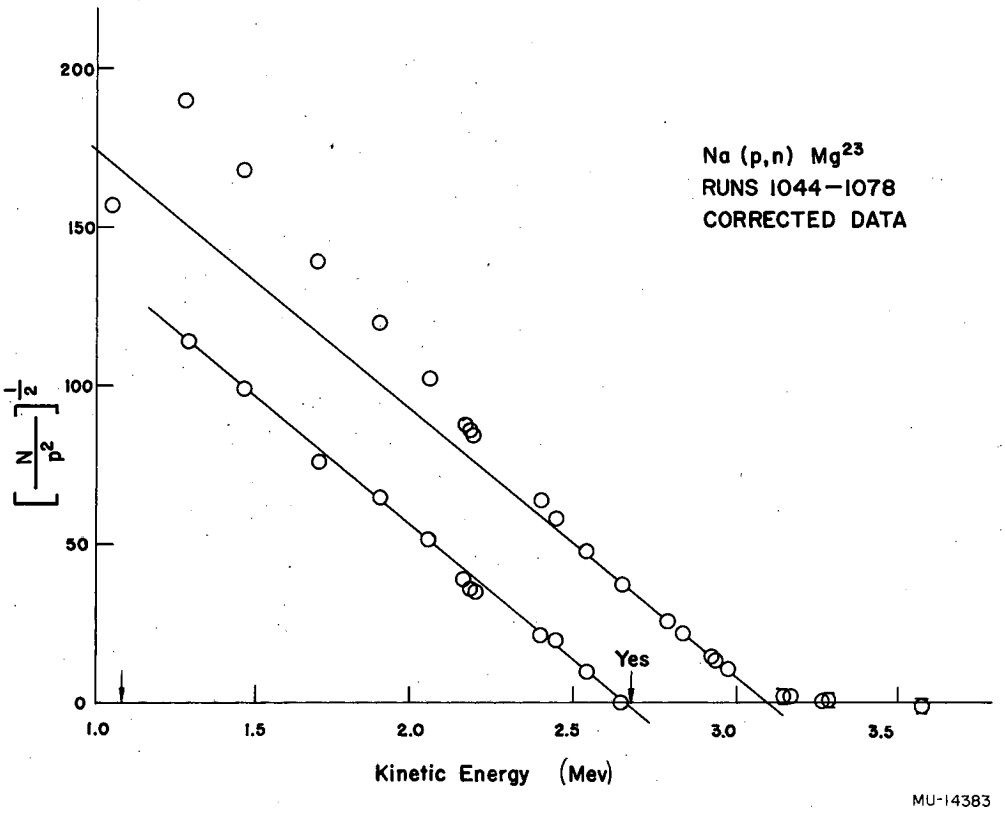

Fig. 10. Kurie plot for Mg^{23}.

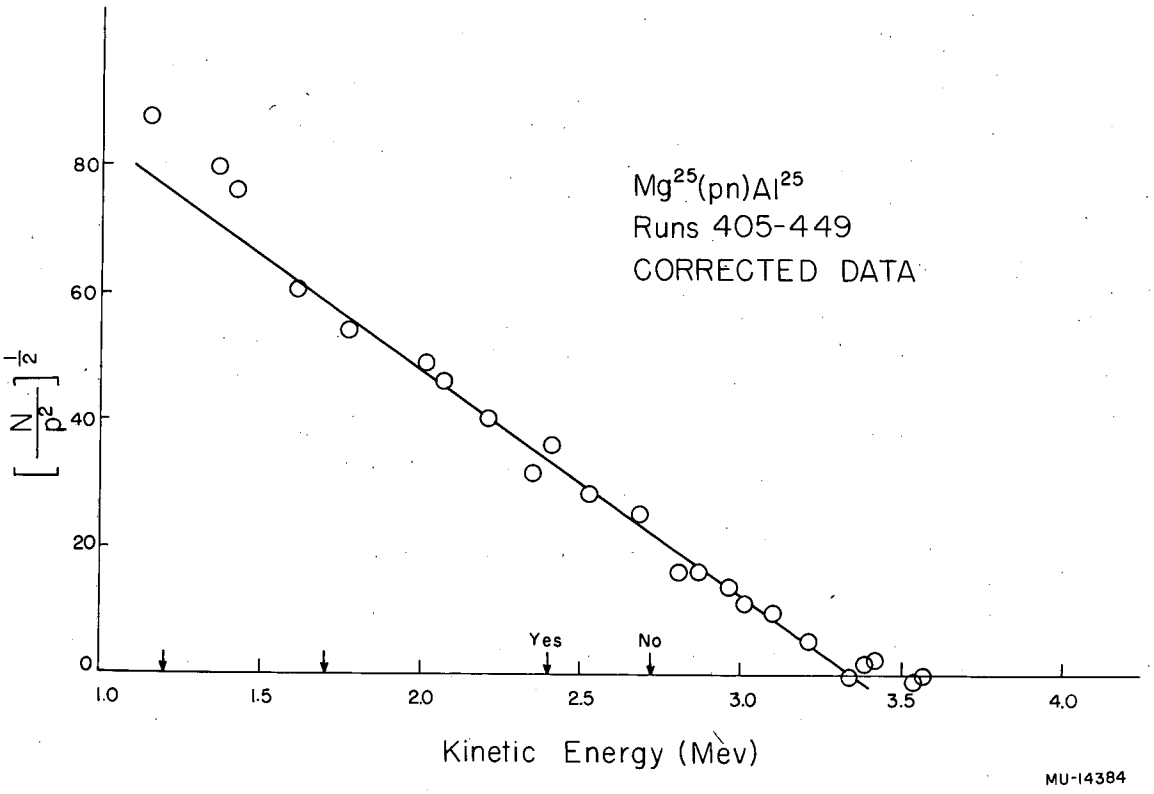

Fig. 11. Kurie plot for Al^{25}. Note the absence of branching transitions.

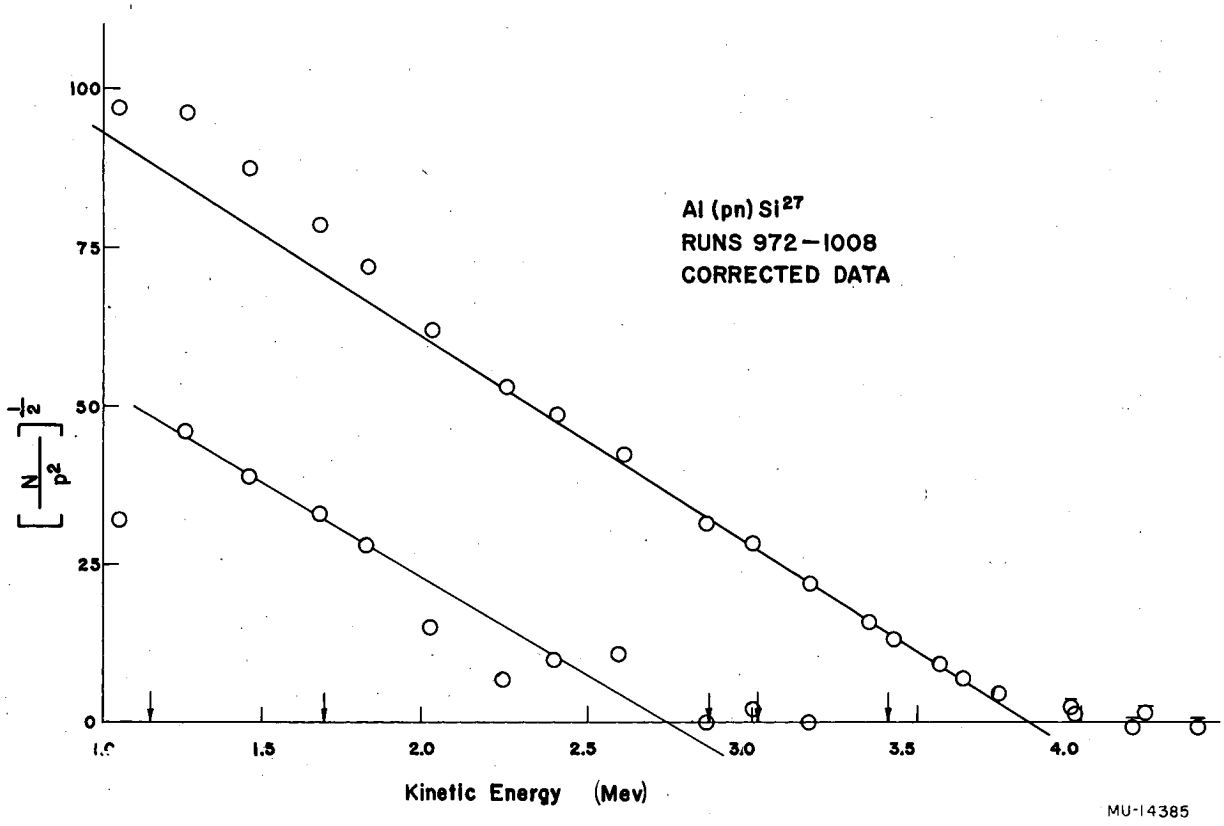

Fig. 12. Kurie plot for Si^{27}.

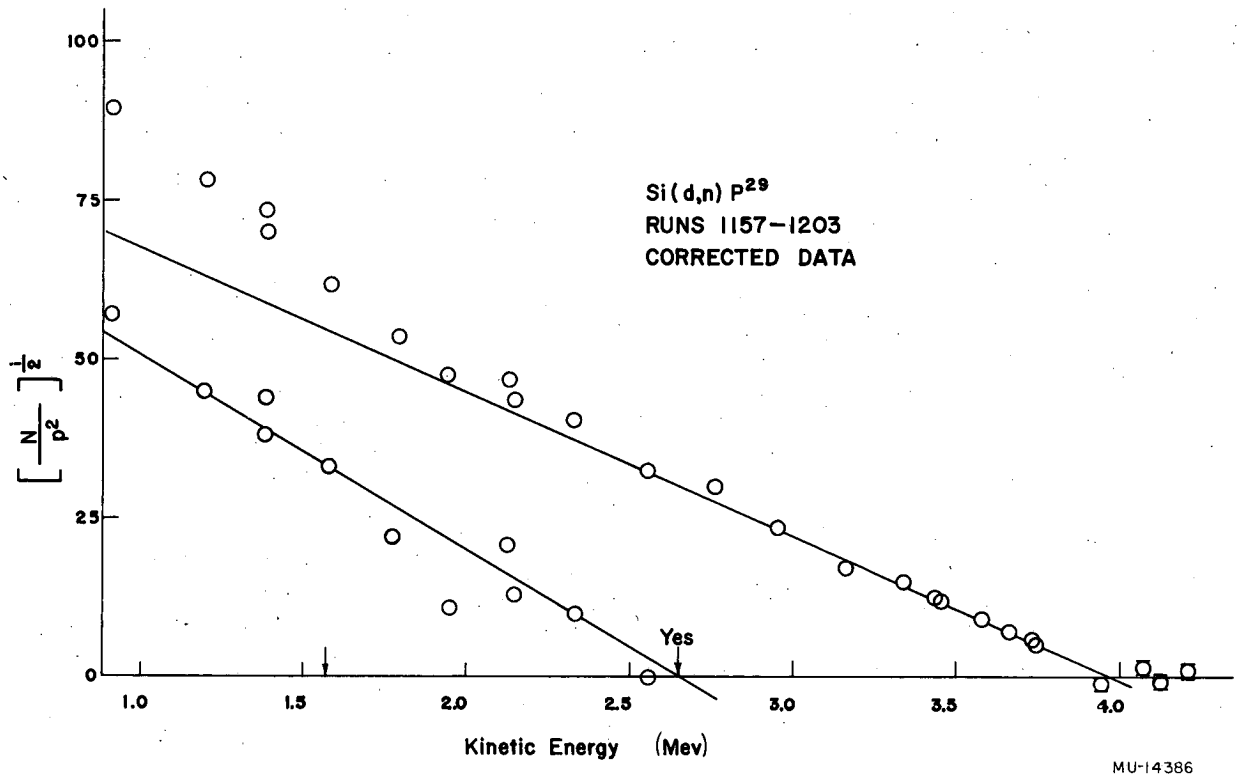

Fig. 13. Kurie plot for P^{29}.

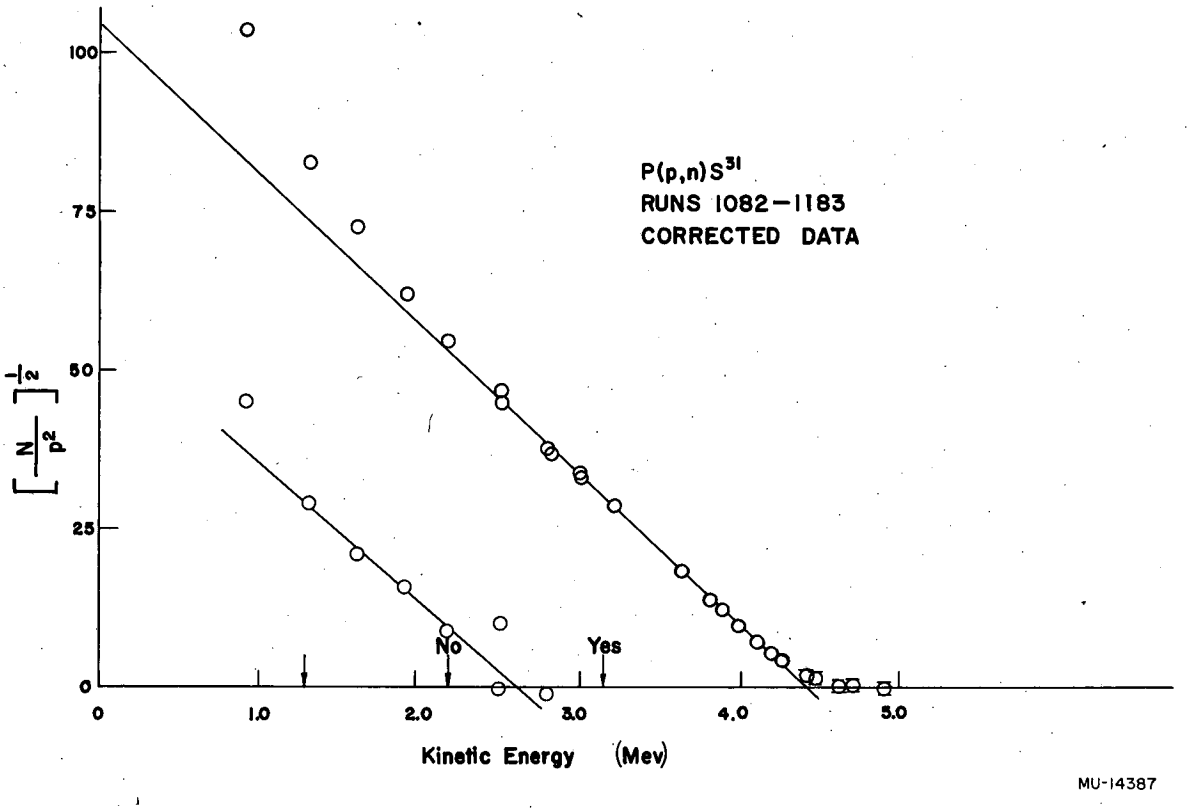

Fig. 14. Kurie plot for S^{31}.

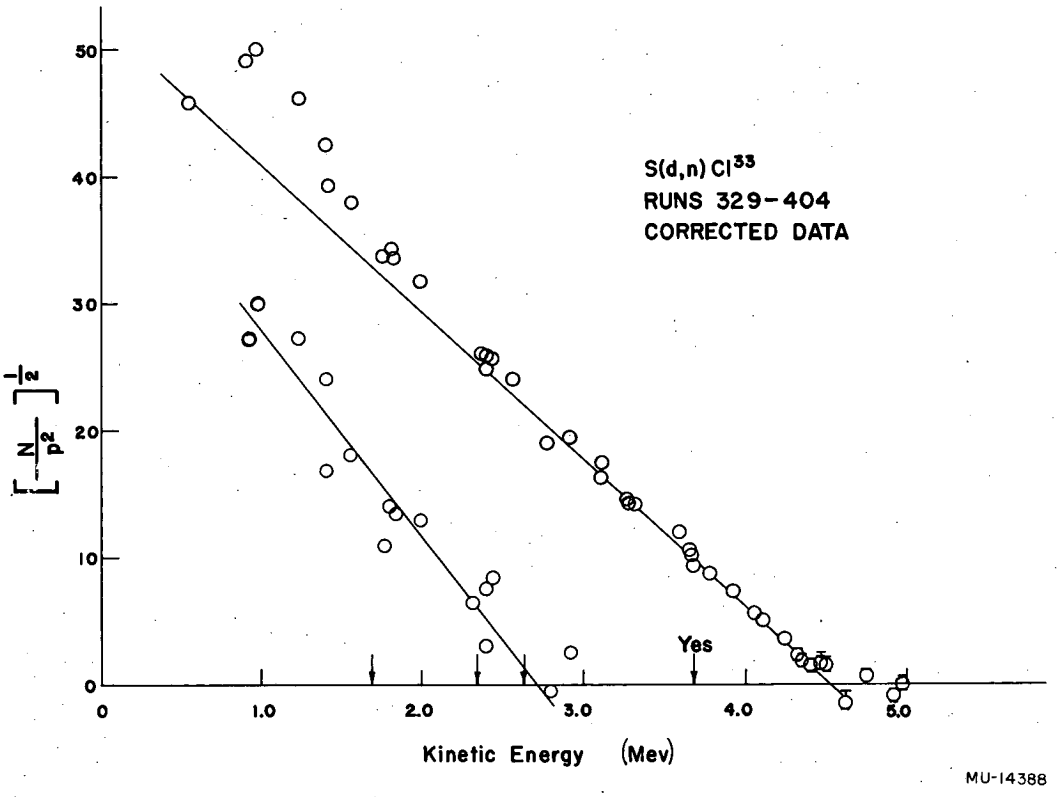

Fig. 15. Kurie plot for Cl^{33}.

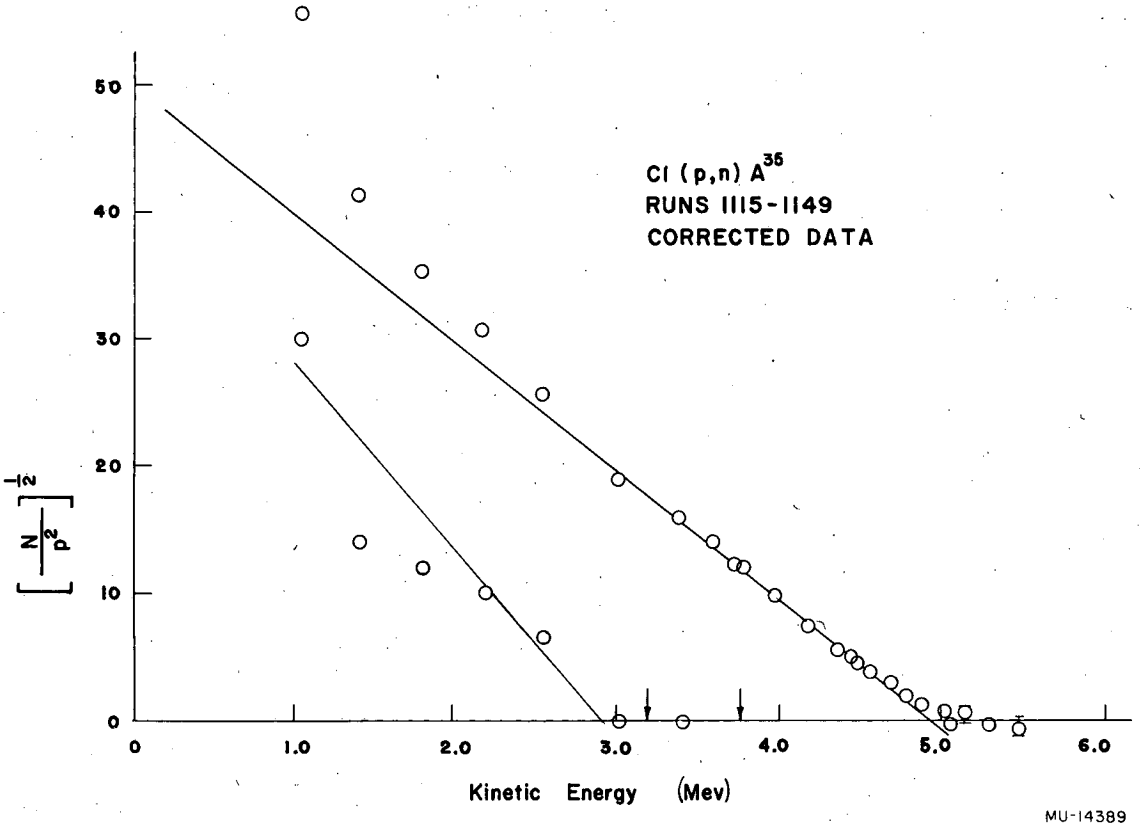

Fig. 16. Kurie plot for A^{35}.

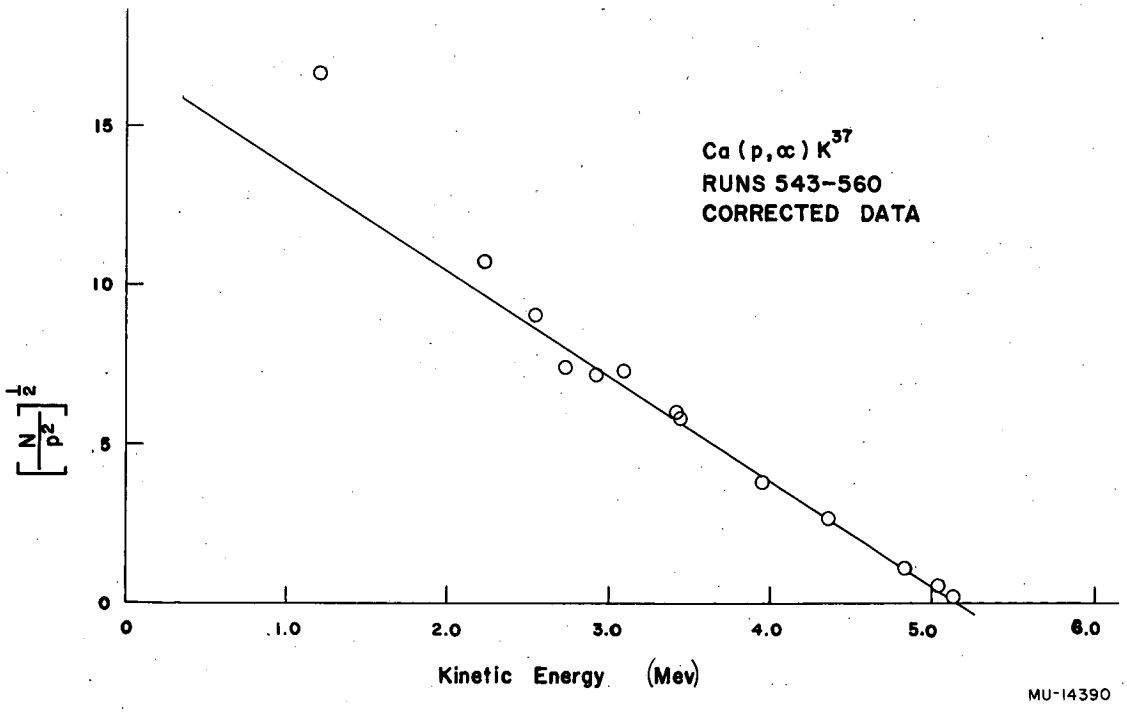

Fig. 17. Kurie plot for K^{37}. The data did not warrant resolving into components.

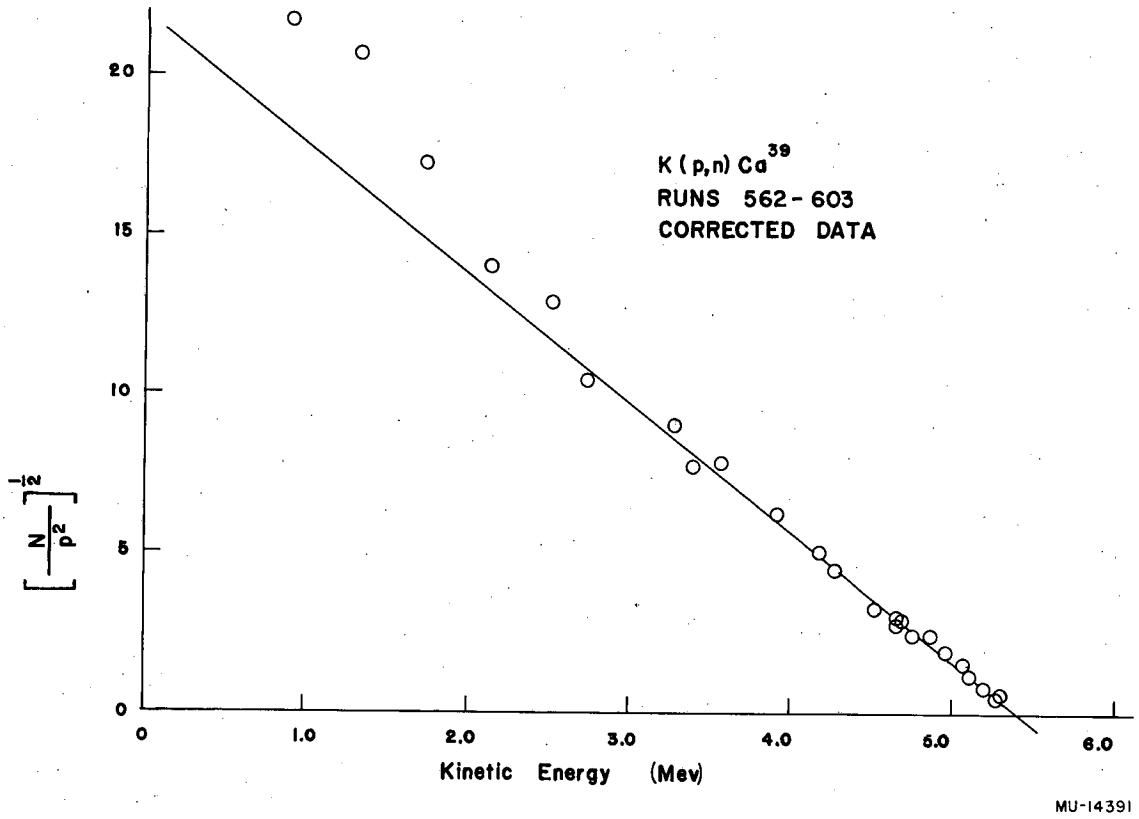

Fig. 18. Kurie plot for Ca^{39}. The data did not warrant resolving into components.

and branching ratio for the next β^+ energy group below the ground-state group was made by resolving the Kurie plot into just two components (see Figs. 8 through 18) wherever there were sufficient data. This is really somewhat tenuous, owing to the counting statistics on the total Kurie plot and our lack of precise knowledge of the efficiency correction. However, in most cases correlation can be found with positions of known levels and spin-parity assignments of the daughters.

Our estimates of branching ratios to be made in Section III-D indicate that only transitions obeying allowed selection rules ($\Delta J=0, 1$; no parity change) will have a large enough branching ratio to be observed as a bend in our Kurie plots.

In Table III we list known energy levels, with spin and parity assignments where known, for the daughter isobars of the mirror transitions. The column headed "Predicted" says "Yes" for allowed transitions, "No" otherwise. The column headed "Reported" lists results of other β-spectra measurements. The column headed "Observed" gives the results of this experiment. At the bottom of each rectangle is given any information on γ rays. For the most part the pattern fits; there are, however, some discrepancies:

F^{19} We see evidence for a transition to a hitherto unreported state at 0.5 ± 0.2 Mev (see Ne^{21}).

Ne^{21} We do not see a branch to the 0.35-Mev level. Schrank's and Richardson's work[33] sheds no light on this and the F^{19} level, as they could see only branching to higher energy levels. Our measurements, Ne^{19} - F^{19} and Na^{21} - Ne^{21}, were taken with comparable source thicknesses, and thus it is hard to see why the F^{19} level is not real; however, the level was not observed by either Freeman[37] or Seale[38].

Mg^{25} We see no branch to the 0.98-Mev level, and no γ rays have been observed from this level.[43] The spin-parity assignment is not absolutely clear-cut,[52] but does look reasonable.

S^{33} Neither we nor Meyerhof[48] found a branch to the 0.84-Mev level.

Table III. Branching transitions to excited states. Each block presents the following data for the daughter isobar shown in its upper left-hand corner: under E, the energy of each known excited state (in Mev); under J, the spin and parity assignment where known; under Pred., Reptd., and Obs., whether a significant branching transition to each listed level is predicted according to the spin and parity assignments, reported by other experimenters and observed in this experiment, respectively. At the bottom of each block is given any information known about gamma rays. References are enclosed in ( ) and are found in the column so labeled.

Table III

Branching Transitions to Excited States

	Ref.[a]	E	J	Pred.	Reptd.	Obs.
F^{19}	(34)	0	1/2+	Yes	Yes	Yes
		0.109	1/2-	No		
		0.167	5/2+	No		
		1.342	3/2			
		1.452				
		1.551	(3/2+)	(Yes)		
		0.5 + -.2			No	Yes
	(33) no γ's > 0.51 Mev					
Na^{23}	(19)	0	3/2+	Yes	Yes	Yes
	(39)	0.440	5/2+	Yes		Yes
	(40, 41)	2.078				
		2.393				
		2.641				
	(42) no γ's					
Al^{27}	(44)	0	5/2+	Yes		Yes
	(45)	0.442				No
		0.842				at least one
		1.013				
		2.205				
		2.727				
		2.975				
		2.998				
P^{31}	(46)	0	1/2+	Yes		Yes
		1.267	3/2+	Yes		at least one
		2.234	5/2+	No		
		3.133				
		3.293				
		3.414				
Cl^{35}	(49)	0	3/2+	Yes	93%	Yes
		1.221			5%	at least one
		1.763			2%	
	(16)	2.645				
		2.695				
K^{39}	(19)	0	3/2+	Yes		Yes
	(50, 41)	none < 2.0				
	(51)	2.50				
		2.87				

	Ref.	E	J	Pred.	Reptd.	Obs.
Ne^{21}	(35, 36)	0	3/2+	Yes	Yes	Yes
		0.347	3/2+, 5/2+	Yes		No
		1.73	$\leq$ 3/2	Yes	No	
		2.80	1/2	Yes	No	
	(37, 38)	3.73	$\leq$ 5/2	Yes	No	
	(33) no γ's > 0.51 Mev					
Mg^{25}	(19)	0	5/2+	Yes	Yes	Yes
		0.58	1/2+	No		No
		0.98	(3/2+, 5/2+)	Yes		No
		1.61				Maybe
		1.96	(3/2+, 5/2+)	Yes		
		2.56				
	(43) no γ's except 0.51 Mev					
Si^{29}	(19)	0	1/2+	Yes	98.8%	Yes
		1.28	3/2+	Yes	0.8%	Yes
		2.03	(3/2+, 5/2+)	(Yes, No)	< 0.15%	
	(15)	2.43	3/2+	Yes	0.25 ± .15%	
S^{33}	(47, 19)	0	3/2+	Yes	Yes	Yes
		0.844	1/2+	Yes	No	No
		1.966				at least one
		2.312				
		2.869	(5/2-, 7/2-)		1/3%	
	(48)	2.938				
A^{37}	(19)	0	3/2+	Yes		Yes
		1.46				
		1.66				
		2.27				
		2.56				
		3.50				
		4.40				
		4.63				
		5.07				

[a] A level without a reference belongs to the same reference as the level just above it.

Second, there was a long tail on the high-energy end extending well beyond what could be accounted for by spectrometer resolution (see Fig. 19). A review of the data convinced us that it was not due to improper interpretation of the background. We propose rather that the tail arises from positrons that scatter against the walls of the orbit and reach the detector even though they have "too low" a value of $H\rho$. Wong has observed a similar effect and actually showed that the particles contributing to the tail have a wide range of energies below that for which his spectrometer was set, thus indicating that they must have been scattered into the detector.[53] Also from our efficiency-versus-energy data (Fig. 6) we see that the points for each isotope that correspond to this tail (i.e., above the indicated end points) have an efficiency that is characteristic of a much lower energy. For the final analysis, we subtracted off the tail in an empirical manner. We used as a guide some calculations of the effect on a Kurie plot of adding a small, constant amount to the momentum spectrum at every energy. The tail correction had the effect of lowering the Kurie plot intercept 1% to 2%.

The effect of the finite resolution of the instrument and the finite source thickness was obtained by making a folded integral over an allowed spectrum.

We calculated the spectrometer line shape from geometrical considerations. The basic two-dimensional "line shape" for 180° instruments has a sharp edge on the large-radius side and a long tail at small radius. However, the relatively large angular aperture in the direction parallel to the magnetic field and the generally large resolution width acted to produce a spectrometer line shape that was very nearly a symmetric triangle. What asymmetry there was produced only a 0.1% displacement of the apparent end point. Accordingly, for simplicity, for most calculations a symmetric triangle was used.

For an estimate of the maximum source-thickness effect, we chose the source thickness to be a rectangle extending down from the spectrometer setting by one source thickness (in terms of the energy loss of minimum-ionizing electrons).

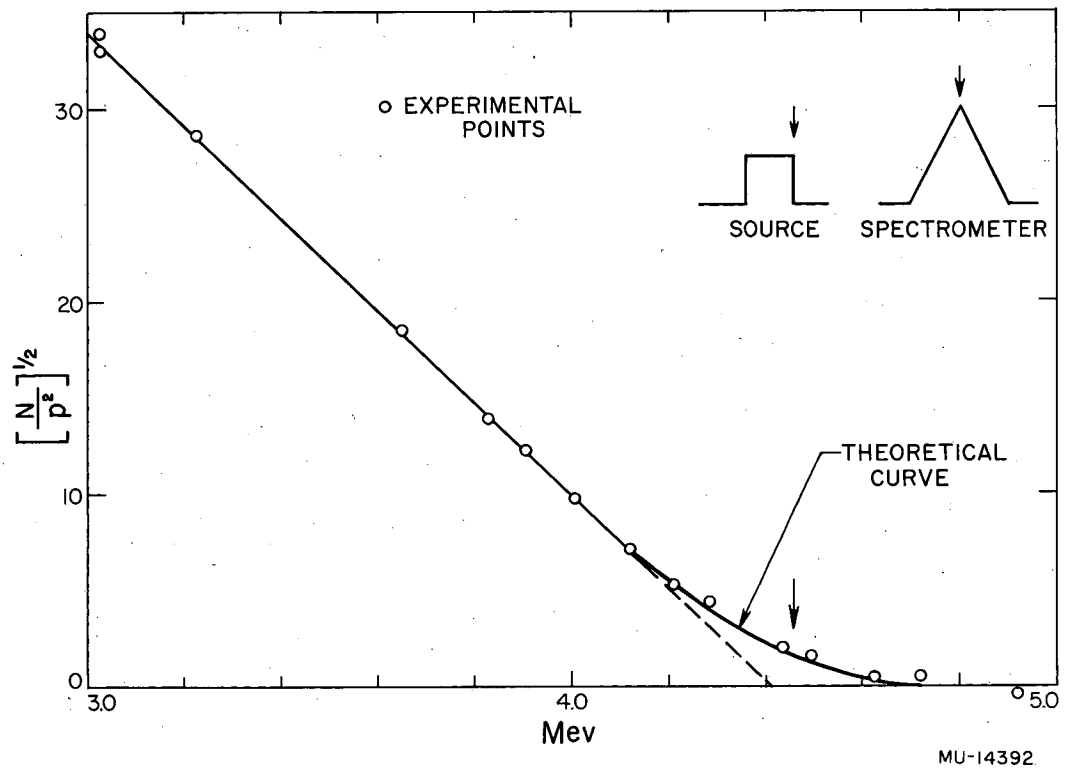

Fig. 19. Effect of finite resolution. The solid curve is computed on the basis of the illustrated resolution shapes and fitted to the experimental points shown. The dashed curve is an extrapolation of the linear portion of the solid curve and is seen to intercept the axis at one-half source thickness below the true end point, whose position is indicated by the arrow.

These shapes and a typical result are depicted in Fig. 19 and fitted to one set of experimental points. The general results are:

(a) the Kurie plot remains straight within our experimental error in the ordinate, over at least the upper two-thirds of the spectrum,

(b) the apparent intercept lies one-half the source thickness below the "correct" intercept, and

(c) the departure from linearity at the high-energy end is confined to a region twice the base resolution width.

We checked the effect of varying source thickness with aluminum targets. The results shown in Fig. 20 indicate that the right correction is probably closer to one-fourth the source thickness. Some of this difference occurs because the rear portions of thick targets are not activated as highly as the front portions, owing to the decreasing cross section as the incident protons or deuterons lose energy. Thus the correct source-thickness shape is skewed toward the actual spectrometer setting.

We chose to correct by one-third of the target thickness, and feel that this choice introduces an error no larger than 10% (0.01 Mev) of the source thickness in the end-point energies.

All corrections have been applied to the data presented in Figs. 8 through 18.

That portion of each Kurie plot which lies above the last known level of the daughter, and (or) that portion which is observed to be straight were fitted by least squares to determine the end-point energies and errors presented in Table IV. On the whole, the experimental points lie within counting statistical error of the fitted line; occasional points were found to deviate many times as much. These large deviations are attributed to scaler malfunction or recording error, and have been omitted on the plots. Several obvious examples of each were detected when the experiment was performed.

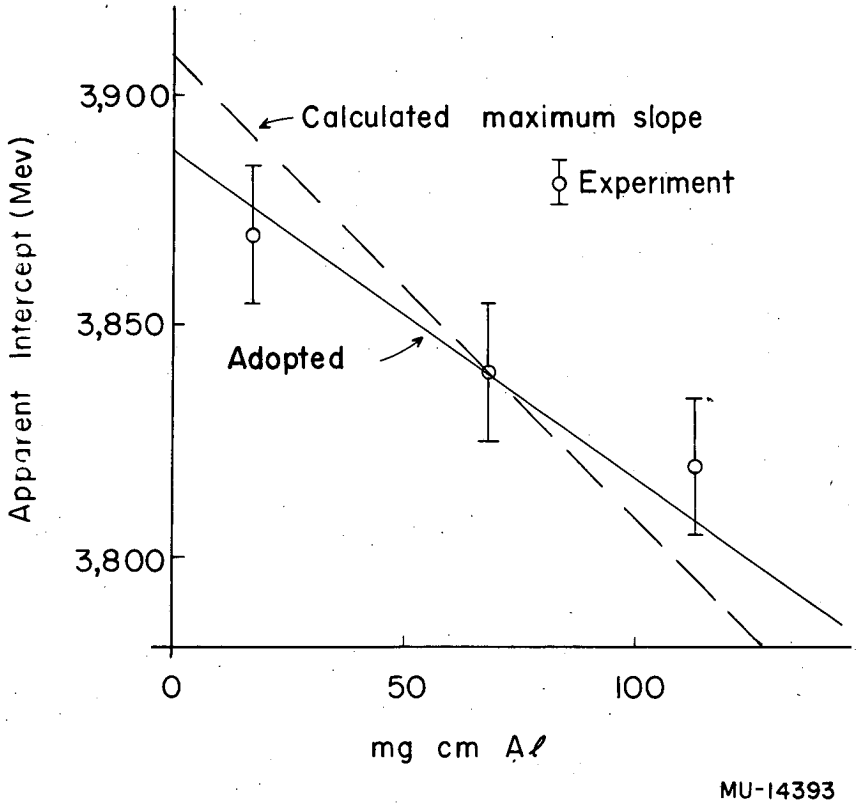

Fig. 20. Source-thickness effect. Experimentally observed intercepts for three source thicknesses are shown together with the maximum calculated thickness effect (dashed curve) and the adopted correction (solid curve).

D. Values of ft

From our energy and half-life measurements we have computed ft values according to the formulas of Feenberg and Trigg.[25] These are really only upper limits, however, as we did not measure branching ratios to excited states of the daughter nuclei, nor are they available, for the most part, in the literature. One can estimate the uncertainty introduced as follows. A branching transition could meet the allowed selection rules but would not have so large a matrix element as the ground-state transition that is between analogue states. The expected minimum log ft is ~4.7 (i.e., maximum transition probability) for such transitions. Contrast this to a maximum log ft $\cong$ 3.7 for the mirror transitions. From our survey of excited levels, Table III, we find that the first level occurs 0.5 to 1 Mev above ground state. The branching ratios for typical combinations are

Ground-state energy (Mev)	% to 0.5-Mev level	% to 1-Mev level
3.0	4.8	2
5.0	5.6	2.5

The few experimental measurements[15, 16] confirm these estimates. Our ft values are good only to about 10%, so that it is probably not serious to omit a branching-ratio correction.

E. Errors

1. Energies

The basic magnetic-field measurements are accurate to 0.1% absolutely; corrections for deviations from a uniform field push the absolute error for the effective field to 0.4%, and the relative error to 0.2%. The position and spatial uniformity of the beam were controlled by collimation and burn-pattern analysis so as to introduce an error in the effective source position no larger than 0.015 inch absolutely. This produces a 0.2% error in the effective radius of the orbit. Thus the basic accuracy in the Hρ of the instrument is 0.5%

absolutely and 0.3% relatively.

The previously discussed source-thickness error is 0.01 Mev, or 0.5% to 0.2%, depending on the energy.

The internal accuracy of individual Kurie plots varied from 0.3% to 1.5% for the ground-state transitions. This is compatible with counting-statistics errors, indicating no appreciable contribution from beam monitoring, or from the shape of the detection-efficiency curve.

The combined relative error from internal fit, source thickness, and $H\rho$ is given in Table IV.

Every isotope was measured at least twice, and from two to eight spectra were determined during each of nine runs performed over a 10-month period. Many cross checks are thus available, and all runs for the same isotope agreed within the accuracy of the individual measurements.

2. Half Life

The entire error in the half life comes from uncertainty in the correct background-counting rate, as our timing gear was accurate to 0.1%.

3. Values of ft

The error in ft values was compounded from absolute energy and half-life errors, based on $ft \propto E^5 t$ for this region of energies. No allowance was made for possible branching ratios. That is, we give in Table IV the upper-limit value of ft and the error in this upper limit.

F. Comparison with Other Data

Our half-life determinations agree with those from other experiments as reported by King.[17]

We have chosen to use the Coulomb energy differences for comparison. These are obtained from β decay as

$$\Delta_1 = E_{max} + 2m_0c^2 + (n-p)c^2 = E_{max} + 1.804 \text{ Mev for } \beta^+, \text{ and} \quad (1)$$

$$\Delta_1 = E_{max} - (n-p)c^2 \text{ for } \beta^-; \quad (2)$$

Table IV. Data for mirror nuclei. Column 1 identifies the information presented with the mass number, A_{mp}, of the mirror pairs. Columns 2 and 3 present the half life, $T_{1/2}$, and the maximum β energy, E_{max}, of the mirror transition. P.U.S. indicates the higher Z member is proton unstable; K indicates that the transition is by K-capture. Column 4 gives the computed values for the relative transition probabilities or ft values. Column 5 gives the Coulomb-energy difference of the mirror pair, Δ_1. Column 6 gives the differences, Δ_2, between the values of Δ_1, for successive mirror pairs. The Δ_2 are located on the line in between the values Δ_1, that they connect. Column 7 gives the values of the Carlson-Talmi energy coefficient, $\xi(A_{mp})$.[10] In Column 8 are the experimental values of the characteristic Coulomb energy of the harmonic ascillator well, ϵ_{exp}, defined by $\Delta_1 = \xi(A_{mp})\epsilon_{exp}$. Column 9 gives values of ϵ_π deduced by Talmi and Thieberger's[54] fit of binding energies. The experimental values for $A_{mp} = 19$ through $A_{mp} = 39$ are from this experiment, while the rest are taken from Carlson and Talmi.[10] Errors in this table are to the right of the values given, but in some subsequent tables are immediately above the value.

Table IV

Mirror Nuclei Data

1	2	3	4	5	6	7	8	9
A_{mp}	$T_{1/2}$	E_{max} (Mev)	ft (sec)	Δ_1 (Mev)	Δ_2 (Mev)	$\xi(A_{mp})$	$\epsilon_{exp.}$ (Mev)	ϵ_π (Mev)
1	13 m	0.78	1260	0.0		—	—	
					0.764±.001			
3	12 y	0.018	1150	0.764±.001		2.00	0.382	
					0.04±.30			
5	—	P. US.	—	0.8±.3		3.00	0.270	
					0.85±.30			
7	53 d	K	2340	1.645±.001		4.667	0.352	
					0.207±.002			0.364
9	—	P. US.	—	1.852±.002		5.667	0.327	
					0.910±.004			
11	20.5 m	0.960±.003	3890	2.762±.003		7.333	0.377	
					0.242±.005			
13	10.0 m	1.200±.002	4670	3.004±.002		8.667	0.346	
					0.485±.005			0.349
15	2.1 m	1.685±.005	3860	3.489±.005		10.167	0.343	
					0.060±.008			
17	66±3 s	1.745±.006	2280±100	3.549±.006		10.350	0.3430	
					0.49±.02			
19	19.5±1.0 s	2.24±.01	1900±100	4.04±.01		11.832	0.3387±.0008	
					0.27±.02			
21	21.6±.5 s	2.51±.02	3500±250	4.31±.02		12.643	0.3390±.0017	
					0.58±.02			
23	11.9±.3 s	3.09±.01	4480±200	4.89±.01		14.125	0.3445±.0010	0.349
					0.29±.03			
25	7.3±.3 s	3.38±.03	4280±350	5.18±.03		14.937	0.3449±.0020	
					0.47±.04			
27	4.33±.02 s	3.85±.02	4500±100	5.65±.02		16.418	0.3426±.0007	
					0.09±.03			
29	4.2±.1 s	3.96±.02	4740±200	5.76±.02		18.113	0.3165±.0011	0.320
					0.43±.04			
31	2.58±.6 s	4.39±.03	4820±250	6.19±.03		19.447	0.3166±.0016	
					0.12±.06			
33	2.90±.10 s	4.51±.05	6000±500	6.31±.05		20.098	0.3127±.0025	
					0.42±.07			
35	1.84±.10 s	4.93±.05	5680±400	6.73±.05		21.508	0.3119±.0024	
					0.22±.09			0.312
37	1.15±.15 s	5.15±.07	4250±500	6.95±.07		22.311	0.3104±.0031	
					0.28±.09			
39	0.89±.05	5.43±.06	4150±300	7.23±.06		23.721	0.3035±.0028	
					-0.49±.12			
41	0.87±.05 s	4.94±.10	2180±250	6.74±.10		22.985	0.2932±.0050	
								0.289
43						24.341		

This experiment

from (p, n) thresholds as

$$\Delta_1 = - Q(p, n); \tag{3}$$

and from difference of (d, n) and (d, p) reaction energies as

$$\Delta_1 = Q(d, p) - Q(d, n), \tag{4}$$

where the two reactions lead from a common nucleus to the members of a mirror pair.

A survey of available data is given in Tables V and VI. Table V presents all the previous β measurements. Some of the values are quite divergent, especially the older cloud-chamber results, which appear to be uniformly low, and some of the crystal-scintillometer results, which are high. Our values are quite consistent with the magnetic-spectrometer values, except at $A_{mp} = 19$.

Table VI presents some Q-value measurements together with the "best" previous β-spectra measurement and the results of this experiment. Discounting a recent determination of $A_{mp} = 19$,[55] we agree with all the values from (p, n) reactions except possibly at $A_{mp} = 27$, where our value is just a little too high for the quoted errors to overlap. For the deuteron-reaction differences, our values are higher than 2 and below 2 beyond the reported experimental errors in all cases. However, we should point out the excellent agreement of this method and the β-energy determination for Sc^{41} by Eliot and King.[18]

Table V. Comparison of β-spectra measurements. The data are labeled in the first column by the two nuclei of the mirror pair. The Column "Ref." lists references for other measurements. The method gives the method used, S = magnetic spectrometer, A = absorption, Scin. = crystal scintillometer, CC = cloud chamber. The value and error of the maximum β-ray energy from the given references and from this experiment are listed.

Table V

Comparison of β-spectra measurements

Transition	Ref.	Method	From References Value (Mev)	From References Error (Mev)	This Experiment Value (Mev)	This Experiment Error (Mev)
Ne^{19}-F^{19}	(33)	S	2.18	.03	2.25	.01
	(56)	A	2.3	.1		
Na^{21}-Ne^{21}	(33)	S	2.50	.03	2.51	.02
	(57)	Scin.	2.5	.1		
Mg^{23}-Na^{23}	(58)	Scin.	2.95	.07	3.09	.01
	(59)	Scin.	2.99	.09		
	(42)	CC	2.82	.14		
Al^{25}-Mg^{25}	(60)	A	3.17	.15	3.38	.03
Si^{27}-Al^{27}	(58)	Scin.	3.76	.08	3.85	.02
	(61)	CC	3.54	.10		
	(62)	CC	3.74	.19		
	(59)	Scin.	3.48	.10		
P^{29}-Si^{29}	(15)	S	3.945	.010	3.96	.02
	(63)	Scin.	3.9	.2		
	(64)	CC	3.63	.07		
S^{31}-P^{31}	(58)	Scin.	4.50	.10	4.39	.03
	(18)	CC	3.87	.07		
	(64)	CC	3.85	.15		
	(59)	Scin.	4.06	.12		
Cl^{33}-S^{33}	(63)	Scin.	4.2	.2	4.51	.05
	(64)	CC	4.13	.07		
A^{35}-Cl^{35}	(64)	CC	4.38	.07	4.93	.05
	(65)	CC	4.41	.09		
	(16)	S	4.96	.05		
K^{37}-A^{37}	(14)	S	5.1	.1	5.15	.07
Ca^{39}-K^{39}	(58)	Scin.	6.10	.15	5.43	.06
	(66)	A	6.7	.5		
	(59)	Scin.	5.13	.15		

Table VI. Comparison of Q values with best β measurements. Again the results are labeled with the mass number, A_{mp} of the mirror pair. References are enclosed in brackets. The columns headed Q(d, p) and Q(d, n) give reaction energies for the indicated reactions leading from the nucleus, $N = Z = (A_{mp} - 1)/2$, to the members of the mirror pair, A_{mp}. The column Q(p, n) gives the reaction energy for the (p, n) reaction connecting the mirror pair, A_{mp}; E_{β^+} is the maximum energy of the positron decay connecting the mirror pair, A_{mp}. The three columns labeled Δ_1 give the Coulomb energy differences deduced from E_{β^+} for this experiment and this survey as well as those obtained from the Q values. The relations used are

$$\Delta_1 = - Q(p, n),$$

$$\Delta_1 = Q(d, p) - Q(d, n),$$

$$\Delta_1 = E_{\beta^+} + 1.80 \text{ Mev}.$$

Table VI

Comparison of Q values with best β^+ measurements

A_{mp}	Q(d, p) (Mev)	Q(d, n) (Mev)	Q(p, n) (Mev)	E_{β^+} (Mev)	Δ_1 (given in Mev) From References β^+	Q	this experiment
19			±.005 -4.039 (35)	±.03 2.18 (17)	3.98	4.039	4.04
21	±.006 4.528 (35)	±.05 - .17 (35)	±.005 -4.235 (55)	±.03 2.50 (17)	4.30	4.235 4.70	4.31
23			±.010 -4.879 (19)	±.07 2.95 (17)	4.75	4.88	4.89
25	±.007 5.097 (35)	±.06 .07		±.15 3.17 (17)	4.97	5.02	5.18
27			±.010 -5.610 (35)	±.08 3.76 (17)	5.56	5.61	5.65
29	±.010 6.246 (35)	±.04 .29 (35)		±.005 3.945 (15)	5.75	5.96	5.76
31			±.20 -6.06 (70)	±.10 4.50 (17)	6.30	6.06	6.19
33	6.41 (67)	.25 (35)		4.13 (17)	5.93	6.17	6.31
35				±.04 4.96 (16)	6.76	-	6.73
37				5.1 (14)	6.9	-	6.95
39				-	-	-	7.23
41	±.010 6.138 (68)	±.05 -0.60 (69)		4.94 (18)	6.74	6.74	-

IV. THEORY

A. Classical Theory

The classical formula for the Coulomb energy of Z protons distributed uniformly throughout a spherical volume of radius R is

$$E_c = (3/5)\, Z(Z-1)\, e^2/R, \qquad (5)$$

and the Coulomb energy difference between the mirror pair (Z + 1), Z is

$$\Delta E_c = 6/5\, e^2\, Z/R. \qquad (6)$$

This model has been reported to give radii following the law

$$R = r_o A^{1/3} \qquad (7)$$

with r_o = 1.46 fermis* for all the mirror pairs up to A_{mp} = 43.[71] However, the results of this experiment show clearly (Table VII and Fig. 21) that r_o is far from constant, exhibiting a regular alternation about a general trend from 1.7 fermis at A_{mp} = 7 to almost 1.3 fermis at A_{mp} = 39, and a large jump to 1.5 at A_{mp} = 41.

There are several defects in this simple model. Because of the exclusion principle, the total proton wave function must be antisymmetric in the exchange of two particles, i.e., the protons appear to avoid one another. For a classical estimate of the effect this has on the Coulomb energy we have used a crystal-lattice model. Neutrons and protons were placed in a body-centered cubic lattice (the most tightly packed lattice) such that each proton had all neutrons for its nearest neighbors, and vice versa. Starting with a proton in the center, a fairly spherical structure is attained for Z = 17. With the aid of a Tinkertoy model we calculated that this arrangement leads to a 15% reduction in the Coulomb energy over that given by Eq. (5).

For the Hartree approximation to antisymmetrization of the total wave function, Cooper and Henly[6] give an approximate formula for E_c,

*1 fermi = 10^{-13} cm.

Table VII. The rms radius constant of the charge distribution of a nucleus, r_o, is defined by $R = r_o(A_{mp})^{1/3}$, where $R^2 = 5/3 \langle r^2 \rangle_{av}$. Values of this constant calculated from values of Δ_1, the Coulomb-energy difference between mirror nuclei, are given for several models: uniform charge distribution without exchange-symmetry correction, with the correction, and the shell model of Carlson and Talmi.[10] The values of $\sigma(A)$ used in this model to compute r_o according to the formula, $\Lambda_0 = \sigma(A)/\Delta_1$ are given. Also presented are values of r_o from high-energy electron-scattering data for the isotopes listed.[23, 72]

Table VII

Rms radius constant for various models

A_{mp}	$\sigma(A)$	Uniform model without exchange	Uniform model with exchange	C-T model	Experimental electron scattering	Isotope for electron scattering
1	-	-	-	-	-	-
					2.01	H^2
3	1.260	-	-	1.65	-	-
					1.31	He^4
5	1.593	-	-	2.0	-	-
					1.98	Li^6
7	2.450	1.640	1.24	1.489	1.83	Li^7
9	2.857	1.780	1.42	1.543	1.89	Be^9
11	3.543	1.400	1.16	1.283	-	-
					1.29-1.35	C^{12}
13	4.023	1.460	1.23	1.341	-	-
15	4.549	1.409	1.21	1.304	-	-
17	4.477	1.496	1.30	$\pm.003$ 1.261	-	-
19	5.082	1.440	1.27	$\pm.003$ 1.267	-	-
21	5.373	1.449	1.29	$\pm.006$ 1.253	-	-
23	5.928	1.360	1.22	$\pm.002$ 1.218	-	-
					1.30-1.33	Mg^{24}
25	6.186	1.365	1.23	$\pm.006$ 1.201	-	-
27	6.706	1.320	1.20	$\pm.002$ 1.192	-	-
					1.28-1.29	Si^{28}
29	7.297	1.365	1.25	$\pm.004$ 1.272	-	-
31	7.727	1.329	1.22	$\pm.006$ 1.252	-	-
					1.28-1.30	S^{32}
33	7.878	1.350	1.24	$\pm.009$ 1.253	-	-
35	8.320	1.326	1.23	$\pm.008$ 1.240	-	-
37	8.520	1.335	1.24	$\pm.012$ 1.230	-	-
39	8.944	1.331	1.24	$\pm.010$ 1.241	-	-
					1.27-1.28	Ca^{40}
41	8.562	1.475	1.37	$\pm.018$ 1.270	-	-
43	-	-	-	-	-	-

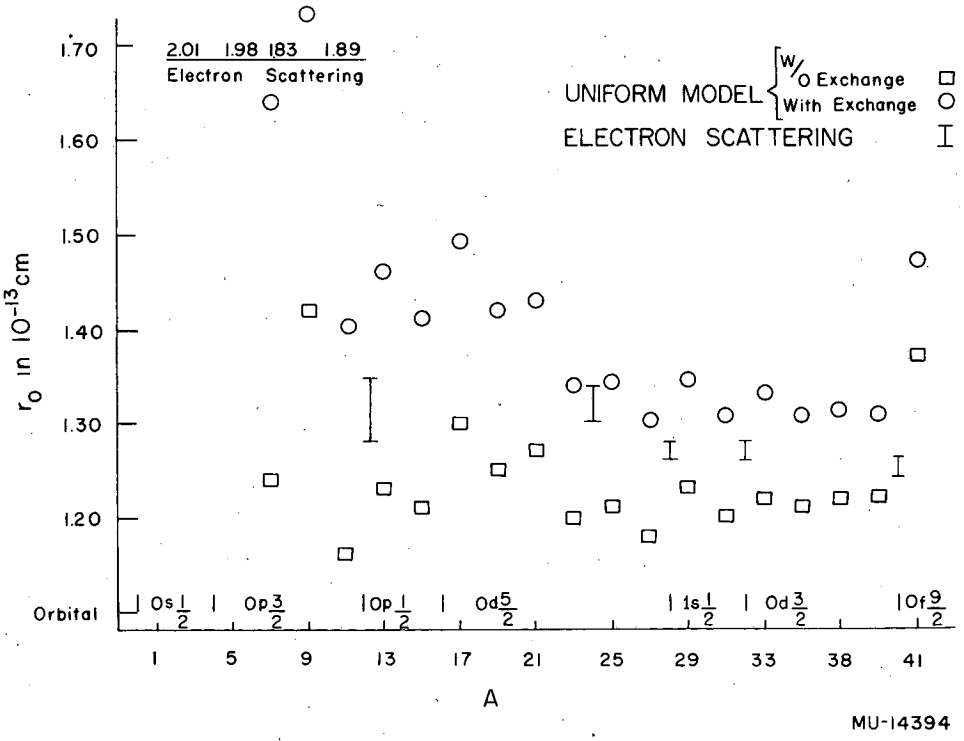

Fig. 21. Rms radius constant versus A_{mp} and orbital of odd nucleon. Values are shown that are based on the uniform model with and without the Hartree-approximation exchange term. The ordinate, r_0, is defined by $R = r_0 (A_{mp})^{1/3}$, $R^2 = 5/3 \langle r^2 \rangle_{av}$. Results from high-energy electron scattering are shown for comparison.

$$E_c \cong 3/5\ Z(Z-1)\frac{e^2}{R} - 0.46\ Z^{4/3}\frac{e^2}{R}; \qquad (8)$$

the first term is called the direct Coulomb energy and the second is called the exchange term, because of the form of the integrals from which they arise. This formula predicts a reduction over Eq. (5) of 12.3% for Z = 17, quite close to the lattice-model reduction. The resulting values of r_o for this model can be obtained from the formula

$$r_o = r_o'(1 - 0.51\ Z^{-2/3}), \qquad (9)$$

where r_o' is the value deduced from Eq. (5); the values are given in Table V and Fig. 21. These values of r_o have no appreciable long-term trend with A, as was pointed out by Peaslee,[12] but do exhibit significant fluctuations from the mean. These fluctuations have been the objects of careful consideration[10] and will be discussed in detail later.

Another defect is the tacit assumption made in going from Eq. (5) to (6) that the radii of the two charge distributions are the same. That is, the protonic charge carried away in the β decay comes uniformly from over the entire charge distribution. The nuclear shell model clearly implies that to the contrary the "disappearing" proton comes from a definite state with a nonuniform probability distribution. For an estimate of this effect, consider that the charge density remains constant, so that the charge contained in the outermost spherical shell volume V, where

$$V = \frac{4\pi}{3}\frac{R^3}{Z+1}, \qquad (10)$$

is carried away. For this model we calculate a reduction in E_c for Z = 10 to 20 over Eq. (6) of 15%. Loss of a proton from the center of the charge distribution would have a correspondingly larger E_c. This additional correction is also implied for a model including the exchange term.

The foregoing discussion is intended to show the necessity for comparing mirror-nuclei Coulomb energies with a detailed theoretical cal-

culation.

B. Symmetry Effects

The first detailed analysis of the symmetry effects in nuclear Coulomb energies was made by Feenberg and Goertzel,[1] and is here reviewed briefly because their model allows us to carry out the analysis in the open without resort to more powerful and hence more obscuring methods necessary for sophisticated models. They used the supermultiplet theory, in which the ground-state wave function is characterized by maximum orbital symmetry and the total proton spin is a good quantum number of value 1/2 for Z odd and 0 for Z even. That is, we have a maximum number

$$N_p = \left[1/2\ Z\right] \tag{11}$$

(where square brackets indicate the largest integer not exceeding the enclosed quantity) of protons paired off with oppositely directed spins. We have

$$N_t = 1/2\ Z\ (Z-1) \tag{12}$$

for the total number of proton-proton bonds, of which N_p are space-symmetric and spin-antisymmetric, and $N_t - N_p$ are "statistical bonds," being 3/4 spin-symmetric and space-antisymmetric and 1/4 spin antisymmetric and space-symmetric, according to the statistical weights of the spin-triplet and spin-singlet states. Therefore if L_s is the Coulomb energy of a pair of space-symmetric protons and L_a that for a space-antisymmetric pair, the total Coulomb energy can be written

$$\begin{aligned} E_c &= N_p\ L_s + (N_t - N_p)\ (3/4\ L_s + 1/4\ L_a) \\ &= 3\,\frac{N_t L_s}{4} + \frac{N_p (L_s - L_a)}{4} = 1/2\ Z(Z-1)\,L_1 + \left[1/2\ Z\right]\ L_2, \end{aligned} \tag{13}$$

defining L_1 and L_2. We expect the last term of the last equality to be positive because of the inherently larger overlap of the space-sym-

metric wave functions. Assuming for the moment that L_1 and L_2 are slowly varying functions of Z, we may express first and second differences in Z in terms of their average values:

$$\Delta_1(Z) = E_c(Z) - E_c(Z-1) = (Z-1)\overline{L}_1 + 1/2 \left[1 + (-1)^Z\right] \overline{L}_2, \quad (14)$$

$$\Delta_2(Z) = \Delta_1(Z) - \Delta_1(Z-1) = \overline{L}_1 + (-1)^Z \overline{L}_2 . \quad (15)$$

Thus we see that the second differences alternate between $L_1 + L_2$ and $L_1 - L_2$. In fact, the data show an alternation of this type, but of a magnitude that itself has rapid variations with Z(Fig. 22). This is really not unexpected, because the values of the L's clearly depend on the exact form of the wave functions, which the supermultiplet theory does not fully determine.

C. Shell Model

Let us then make further assumptions about these wave functions and proceed. We shall use the shell model and define Z' as the number of protons outside closed shells. Then let us write the total Coulomb energy as the sum of three terms: the interaction within the closed shells, the interaction of one outer proton with the entire closed-shell structure, and the interactions among the Z' outer protons, as

$$E_c = \alpha + \beta Z' + \gamma(Z'), \quad (16)$$

and the Coulomb energy difference,

$$\Delta_1(Z') = \beta + \gamma(Z' + 1) - \gamma(Z'), \quad (17)$$

is seen to depend, to an additive constant β, only on the interactions among the outer protons.

Carlson and Talmi[10] point out that the ground state of a mirror nucleus is expected to be predominantly that of lowest seniority.[26] Low seniority is a type of symmetry which implies maximum pairing off of proton spins in LS coupling, or maximum pairing of j in jj

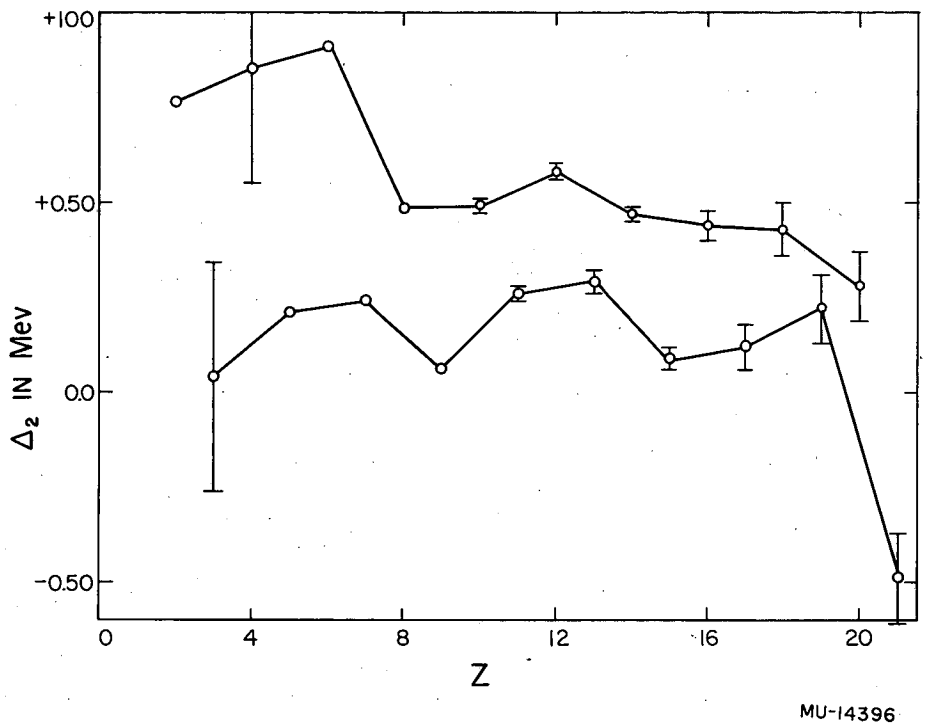

Fig. 22. Second differences with respect to Z of the Coulomb-energy contribution to the total binding energy. The abscissa, Z, x is the highest of the three Z values involved in the differencing. Note the clear odd-even effect throughout and the quantitative interruptions of this effect after Z = 8, 14, 16, and 20.

coupling. For this state they give the formula

$$\gamma(Z') = 1/2\ Z'(Z'-1)a + \left[\!\left[1/2\ Z'\right]\!\right] b \rightarrow \left\{ \begin{array}{l} \Delta_1 = \beta + Z'a + \dfrac{\left\{1 + (-1)^{Z'+1}\right\}}{2} b \\ \Delta_2 = a + (-1)^{Z'+1} b \end{array} \right\}. \quad (18)$$

Here a and b are not quite the L's of Feenberg and Goertzel because of the additional symmetry requirements of low seniority. However, a and b do not depend on Z'; they do depend upon the choice of jj or LS coupling, the ℓ or j of the level being filled, and the radial form of the wave functions.

Carlson and Talmi[10] have made detailed calculations along the above lines for jj coupling, using single-particle wave functions which are stationary states of an isotropic harmonic oscillator well,

$$V(r) = 1/2\ m\omega^2 r^2 = \pi\omega\tau r^2, \quad (19)$$

which has a characteristic energy

$$\epsilon \equiv e^2\sqrt{\frac{\tau}{\pi}}\ . \quad (20)$$

The Coulomb energy is calculated as a perturbation to first order and is found to be a numerical multiple of the characteristic energy of the oscillator ϵ,

$$\Delta_1 = \xi(A)\ \epsilon, \quad (21)$$

where ξ (A) can be evaluated analytically for the harmonic oscillator well.

The experimental values that we obtain for the characteristic energy are given in Table IV and Fig. 23.

The model does not account for the large even-odd alternation in the $p_{3/2}$ shell, but for higher levels the value of ϵ within a shell is remarkably uniform. We use the notation by Carlson and Talmi (C-T) for level order and names -- $0s_{1/2}$, $0p_{3/2}$, $0p_{1/2}$, $0d_{5/2}$, $1s_{1/2}$, $0d_{3/2}$, $0f_{1/2}$.

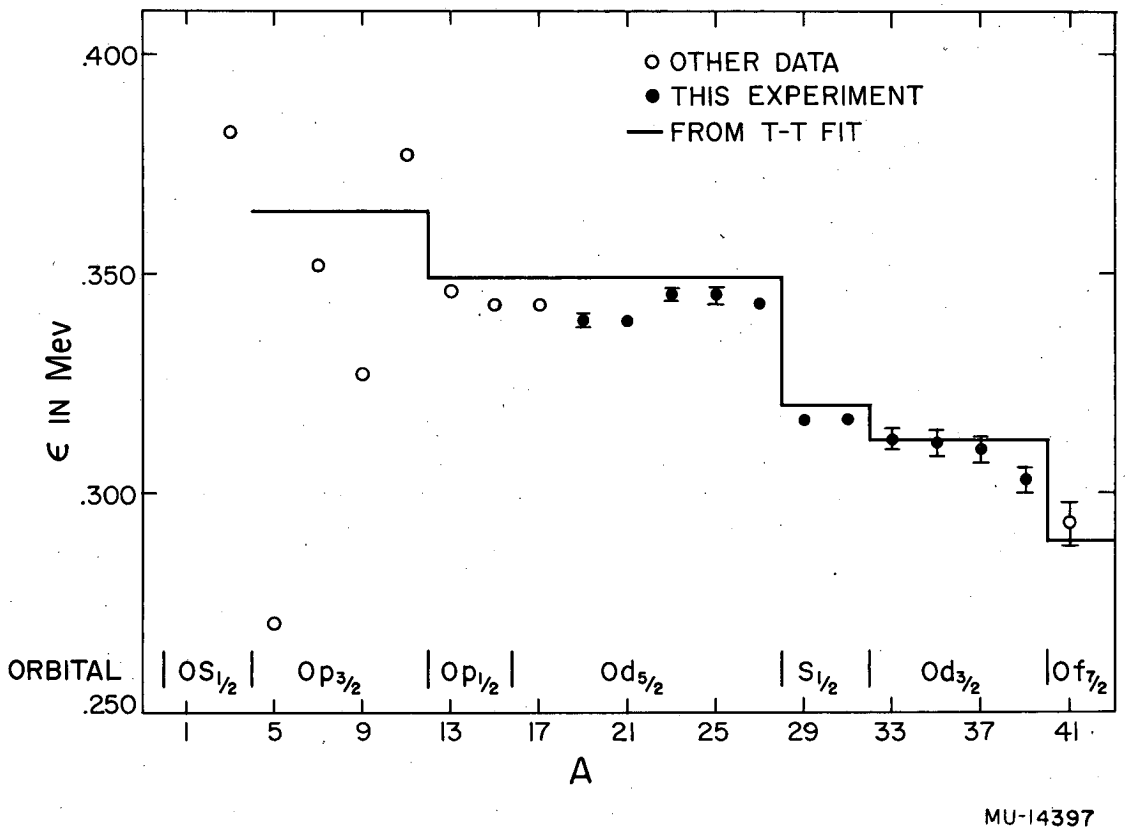

Fig. 23. Characteristic Coulomb energy of the harmonic-oscillator well, ϵ, versus A and orbital of the odd nucleon. This energy is defined by $\epsilon = e^2 (\nu/\pi)^{\frac{1}{2}}$, $V(r) = \hbar \nu r^2$. Note the large alternations in the $0p_{3/2}$ shell, indicating breakdown of the model for extremely small A. The value of ϵ is remarkably constant within the other shells, however. Values of ϵ deduced from a fit of the total binding energies of all known isotopes are shown for comparison.[54]

As a further check of the model we point out the work of Talmi and Theiberger,[54] who developed a five-parameter theoretical binding-energy formula using the C-T theory for the Coulomb energy contribution. This formula was fitted to all known binding energies of light nuclei with rms deviation of 0.1 to 0.9 Mev, depending upon the shell. The values of ϵ so obtained are given in Table III and shown on Fig. 24. The agreement between these values and the values deduced directly from this experiment is excellent. (See Ref. 63 for an extension of this work.)

Even more striking is the uniformity of alternation of the second differences in the $d_{5/2}$ shell (see Fig. 22) and the interruption of the quantitative uniformity at the beginning of each shell above $p_{3/2}$. In Table VIII are presented the average experimental values of the alternation parameter (a-b)/(a+b) together with the computed values for jj and LS coupling for the state of lowest seniority, as well as for an average over all states in LS coupling having the same spin. The $d_{5/2}$ data definitely single out the jj scheme, while the $d_{3/2}$ data are really too inaccurate to discriminate. It is not clear from C-T whether these values for (a-b)/(a+b) would change radically for another type of potential well.

D. Nuclear Radii from Shell Model

Since the experimental Coulomb difference, for given A, determines the spring constant of the oscillator well, it also determines the single-nucleon wave function. In particular, the mean square radius can be obtained directly from the virial theorem. C-T have worked this out to give

$$r_o = \frac{\sigma(A)}{\Delta_1} , \tag{22}$$

where r_o is defined for the equivalent uniform charge distribution as

$$r_o = \left(\frac{5}{3}\right)^{1/2} \left\langle r^2 \right\rangle_{av}^{1/2} . \tag{23}$$

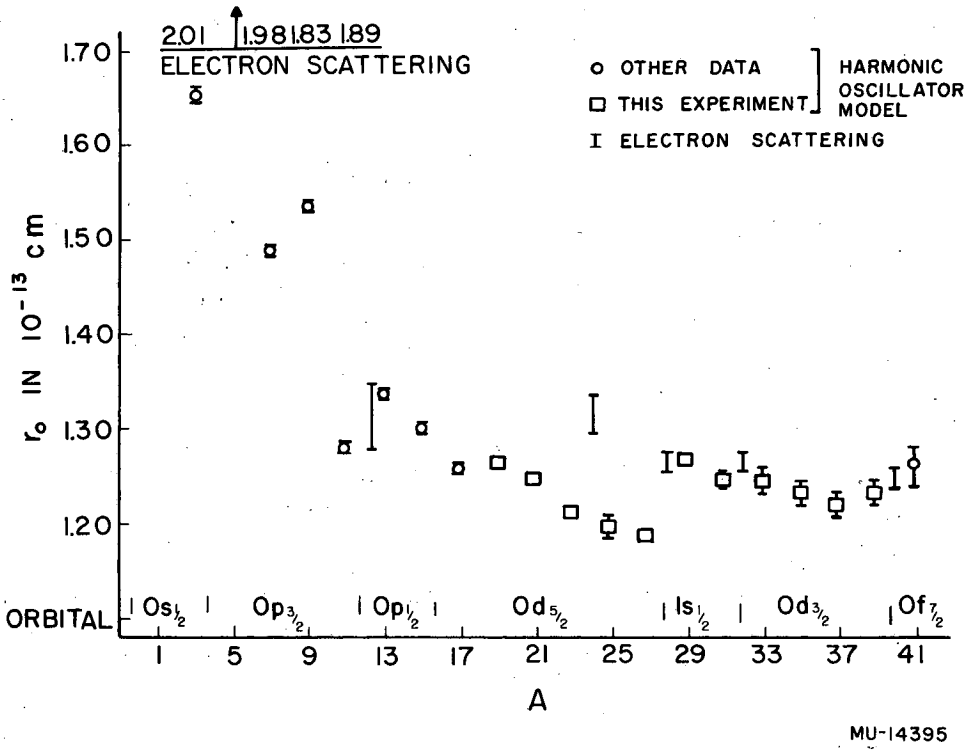

Fig. 24. Rms radius constant versus A and orbital of odd nucleon. Values shown are based on a nuclear shell model using harmonic-oscillator wave functions.[10] The ordinate is defined as in Fig. 21, and again electron-scattering results are shown for comparison.

Table VIII. Pairing effect. The alternation of the second differences, Δ_2, of the nuclear Coulomb energy is presented for the last proton being in a $0d_{5/2}$ orbital (A_{mp} equal to 17 through 27) and being in a $0d_{3/2}$ orbital (A_{mp} = 33 through 39). The values of Δ_2 should alternate between a+b and a-b, and are grouped into columns accordingly. The average value of the alternation parameter, (a-b)/(a+b), is compared with theoretical predictions for various models.

Table VIII

Pairing effect

Odd nucleon in $0d_{5/2}$ orbital

	Δ_2		(a-b)/(a+b)		
			This experiment	Theory	
A_{mp}	a+b	a-b			
17 - 19	±.02 0.49			0.44 for	LS in lowest seniority
19 - 21		±.02 0.27			
21 - 23	±.02 0.58		±.07 0.55	0.55 for	jj in lowest seniority
23 - 25		±.03 0.29			
25 - 27	±.04 0.47			0.83 for	LS averaged over same spin

Odd nucleon in $0d_{3/2}$ orbital

	Δ_2		(a-b)/(a+b)		
			This experiment	Theory	
A_{mp}	a+b	a-b			
33 - 35	0.42±.07			0.44 for	LS in lowest seniority
35 - 37		±.09 0.22	±.25 0.62	0.40 for	jj in lowest seniority
37 - 39		±.09 0.28		0.83 for	LS averaged over same spin

It should be pointed out that the model itself implies that r_o decreases uniformly throughout a shell if ϵ is constant. That is, the alternation of the second differences is all absorbed in the wave-function symmetry and is not reflected as alternations in radii, but there remains an increasing relative compactness as a shell is filled. In principle, there exists a discontinuity in r_o as a shell is started. However, a change in ϵ between shells may just compensate, as for $1s_{1/2}$ and $0d_{3/2}$.

The following viewpoint is proposed. The value of ϵ is a measure of the average nuclear force experienced by nucleons in a particular shell. This is expected to be the same for nucleons having the same wave function -- i.e., in the same shell -- but might be different for different shells. This difference depends explicitly on the exact form of the nuclear force, and goes beyond the assumption and hence predictions of this theory. (The theory does include the variation in Coulomb energy caused by the spatial distribution of states of different angular momentum.) Thus the value of the rms radius of the charge distribution should be considered as a result rather than an input to the model.

Nevertheless, the detailed explanation by the theory of the energies for A_{mp} higher than 12 leads us to believe that the radii computed in this manner are real. Jancovici[9] has shown that a finite square well leads to values of $\sigma(A)$ that are at most 1% different from those for a harmonic oscillator well at A = 15 and 17. The experimental values of r_o from Eq. (22) are given in Table VII and Fig. 24, where they are compared with results from high-energy electron-scattering experiments,[72] which give r_o = 1.3 fermis in this region. These experiments do not measure rms radii directly, and most of the variation included in the errors listed comes from the theoretical interpretation. Therefore we can conclude that the two determinations are substantially in agreement except for the point at A = 24. This is a region where evidences for nonspherical nuclei have been found.[73] Now, the electron-scattering experiments are very sensitive to the shape of the charge distribution near the surface, and any deformation would enter into the average fuzziness of the surface, to first order.

The Coulomb energy necessarily depends on deformation to second order, because it is a minimum for a sphere. Thus we might expect our model to give detailed explanation of energies while being insensitive to actual departures from sphericity.

The radii from μ-meson x-ray determinations are consistent with a constant value for r_o of 1.2 fermis, but the measurements are confined to the region above A = 51. The C-T model, when normalized either to the mirror difference at A = 41 or the fit of T-T, predicts r_o = 1.2 for A = 51. Thus the stated disagreement[19, 22] between the μ-mesonic atom radii and those from mirror nuclei disappears when they are compared with a suitable theory in the correct mass-number region.

E. Coulomb Energy in the Triads

Following the method of Wilkinson[21] we have constructed Table IX. We have used his data for mass differences and T = 1 energy levels for the triads and the data listed in Table IV for mirror pair mass differences. The purpose of this table is to test our assumption of the charge independence of nuclear forces.

In the language of isotopic spin,[74] charge independence implies that there is a state of the self-mirrored member of each triad that has exactly the same set of nuclear wave functions as the ground states of the neutron- or proton-rich members of the triad. That is, there exists a state of $T = 1$, $T_Z = 0$ which is the "analogue state" of the states $T = 1$, $T_Z = 1$. If this is so, then the Coulomb energy difference between analogue states is the total energy difference, aside from the neutron-proton mass difference. For example, we have

$$\left[{}_5B^{10}(T=1) - {}_4Be^{10}(T=1)\right] = \left[{}_5B^{9}(T=1/2) - {}_4Be^{9}(T=1/2)\right](1-1/9)^{1/3},$$

where (a) the bracket on the left denotes the energy difference, corrected for the n-p difference, of the T=1 analogue states for B^{10} and Be^{10}, (b) the bracket on the right is the corresponding difference for the T=1/2 analogue states for B^9 and Be^9 -- i.e., the ground states

Table IX. Coulomb energy in the triads. The first two columns give the energy differences in Mev, corrected by the neutron-proton energy difference, between the ground states of the listed pairs of isobars. In Al^{26} and K^{38} the energy difference to the first T = 1 level is given (see text). These energy differences and the Coulomb energy differences of the mirror pair listed under "Mirror Pair A_{mp}" are used to calculate expected positions of the analogue T = 1 state of the nuclides listed under "nucleus." The calculated and observed positions of these analogue states is given under E(T=1) - E(Gnd). The difference between calculated and observed values is listed under δE. The entries under "calculated" which have no entry under "Mirror pair A_{mp}" on the same line were calculated from theoretical formulae by use of both ground-state energy differences involving the nucleus in question.

Table IX

Coulomb energy in the triads

Isotopes	Ground-state energy difference + (n-p) difference	Mirror pair A_{mp}	Nucleus	E(T=1) - E(ground) Calculated	E(T=1) - E(ground) Observed	δ E
He^6-Li^6	2.77 ± .05	5	Li^6	3.61 ± .02	3.57 ± .01	.04 ± .03
Li^8-Be^8	15.20 ± .04	7	Be^8	16.77 ± .04	16.72 ± .01	.05 ± .04
Be^{10}-B^{10}	- .226 ± .003	9		1.57 ± .01		-.17 ± .01 *
			B^{10}	1.775 ± .027	1.739 ± .003	+.04 ± .03
B^{10} - C^{10}	4.42 ± .06	11		1.56 ± .06		-.18 ± .06 *
B^{12}-C^{12}	12.588 ± .025	11		15.27 ± .03		+.17 ± .04
			C^{12}		15.10 ± .02	
C^{12}-N^{12}	18.4 ± .1	13		15.3 ± .1		+.2 ± .1 *
C^{14}-N^{14}	- .627 ± .001	13		2.302 ± .003		-.011 ± .005
			N^{14}	2.336 ± .004	2.313 ± .004	+.023 ± .007
N^{14}-O^{14}	5.952 ± .008	15		2.388 ± .010		+.075 ± .012
N^{16}-O^{16}	9.62 ± .03	15	O^{16}	13.08 ± .03	12.95 ± .01	+.13 ± .03
O^{18}-F^{18}	- 2.453 ± .009	17		1.029 ± .009		-.046 ± .015
			F^{18}		1.075 ± .010	
F^{18}-Ne^{18}	5.0 ± .2	19		.9 ± .2		-.2 ± -.2 *

Table IX (cont.)

Isotopes	Ground state energy difference + (n-p) difference	Mirror pair A_{mp}	Nucleus	E(T=1) - E(ground) Calculated	E(T=1) - E(ground) Observed	δ E
F^{20}-Ne^{20}	6.261 ± .012	19	Ne^{20}	10.221 ± .015	unknown	-
Ne^{22}-Na^{22}	- 3.623 ± .006	21	Na^{22}	0.61 ± .03	near .592 ± .003	near +.02 ± .03
Na^{24}-Mg^{24}	4.730 ± .005	23	Mg^{24}	9.55 ± .01	9.47 ± .10	+.07 ± .10
Mg^{26}-$Al^{26}_{(T=1)}$	- 5.006 ± .010	25	Al^{26}	5.12-E ± .03	5.01-E ± .01	+.11 ± .03
Al^{28}-Si^{28}	3.868 ± .011	27	Si^{28}	9.45 ± .02	9.27 ± .11	+.18 ± .11
Si^{30}-P^{30}	- 5.08 ± .04	29	P^{30}	.62 ± .04	.688 ± .007	-.07 ± .08
P^{32}-S^{32}	0.925 ± .004	31	S^{32}	7.05 ± .03	7.02 ± .05	+.03 ± .06
S^{34}-Cl^{34}	- 6.30 ± .03	33	Cl^{34}	- .05 ± .05	0	-.05 ± .05
Cl^{36}-A^{36}	- .068 ± .005	35	A^{36}	5.97 ± .06	unknown	-
A^{38}-$K^{38}_{(r=1)}$	- 6.37 ± .13	37	K^{38}	6.99-E ± .07	6.37-E ± .13	+.62 ± .18 *
K^{40}-Ca^{40}	0.543 ± .015	39	Ca^{40}	7.77 ± .06	unknown	-

not counting values marked * , one obtains $\overline{\delta E}$ = +.047 ± .074;

counting all values, one obtains $\overline{\delta E}$ = +.047 ± .172.

$\delta E \approx +.047$ implies n-p bond stronger than n-n bond by $\sim 1.5\%$

of the mirror pair; and (c) the factor $(1-1/9)^{1/3}$ applies a first-order correction to account for the generally larger size, and hence smaller Coulomb energy, of the mass 10 nuclei over the mass 9 nuclei. Subtracting the ground-state energy, ${}_5B^{10}(T=0)$, from both sides and rearranging, we get

$$E_{calc}(T=1) = \left[{}_5B^{10}(T=1) - {}_5B^{10}(T=0)\right]$$

$$= \left[{}_5B^{9}(T=1/2) - {}_4Be^{9}(T=1/2)\right](1-1/9)^{1/3} + \left[{}_4Be^{10}(T=1) - {}_5B^{10}(T=0)\right].$$

Similarly we can get

$$E_{calc}(T=1) = \left[{}_5B^{10}(T=1) - {}_5B^{10}(T=0)\right]$$

$$= \left[{}_6C^{10}(T=1) - {}_5B^{10}(T=0)\right] - \left[{}_6C^{11}(T=1/2) - {}_5B^{11}(T=1/2)\right](1+1/11)^{1/3}.$$

It is from these formulae, and the corresponding ones for other triads, that the values $E_{calc}(T=1)$ in Table IX are obtained. For A = 26 and A = 38 the energy difference between T = 1 analogue states is known directly and therefore the energy of the ground state is carried through just as E.

For some triads all three members are known well enough for calculation of E(T=1) from both the higher- and lower-A mirror pair. In addition, we include (on the middle line) values of E(T=1) for A = 10 and A = 14 which Wilkinson calculated from formulae of C-T. Wilkinson ascribed the disparity between this value for B^{10} and the one from the A = 9 mirror pair to the proton instability of B^{9}. However, he did not go through the calculation for B^{10} based on the A = 11 mirror pair. We find that this gives the same low result, 1.56, for E(T=1), but has no explanation in proton instability. At A = 14 the three values are much closer together, but do not really agree.

These calculated values of E(T=1) are then compared with the observed energy level of a state which has been identified as the analogue

state (see Wilkinson for details of this selection).

With the exception of the trouble at A = 10 and an apparently bad experimental point at A = 38, the values of δE (calc-obs) are essentially zero. This is really quite remarkable when one remembers that δE involves subtraction of energies obtained from a wide variety of experimental techniques. The average value of δE is

$\overline{\delta E} = +0.047 = 0.074$ Mev if the starred values are left out, and

$\overline{\delta E} = +0.047 = 0.172$ Mev for all values.

Wilkinson shows that $\delta E = 0.047$ implies that the n-p bond is 1.5% ± 2.5% stronger than the n-n bond. He further compares this with results of singlet-state scattering experiments which imply that the n-p bond is ~3% stronger than the p-p bond. J. Schwinger has suggested that small effects of this size may be due to the different interactions of the nucleon's intrinsic magnetic moments.[75]

Thus the available triad data support the assumption of nuclear equivalence of the analogue ground states of the mirror nuclei.

F. ft Values and Nuclear Matrix Elements

The transition probability of a β transition is given by Fermi's theory[76] as

$$\lambda = \frac{\ln 2}{t_{1/2}} = \left[g_F^2 \left| M_F \right|^2 + g_{GT}^2 \left| M_{GT} \right|^2 \right] f(Z, E_p), \qquad (24)$$

where f denotes an integral over the spectral shape that depends on the maximum energy, the charge of the daughter nucleus, and the sign of the emitted β particle, g_F is the partial-coupling constant for Fermi interaction, g_{G-T} is the partial-coupling constant for Gamow-Teller interaction, and the g's as written here both include a factor $(m^5 c^4)/(2\pi^3 \hbar^7)$, $\left|M_p\right|^2$ and $\left|M_{GT}{}^2\right|^2$ denote the nuclear matrix elements for Fermi and Gamow-Teller interactions respectively. Therefore, we might expect to put the relationship in the form

$$(ft)^{-1} = \left[g_p^2 \left| M_p \right|^2 + g_{GT}^2 \left| M_{GT} \right|^2 \right], \qquad (25)$$

and proceed to evaluate the natural constants g from the experimental ft values and theoretical matrix elements; attempts have been made with great lack of success[77, 27]. For mirror transitions we have $|M_F|^2 = 1$ on the basis of any reasonable coupling scheme. If this is so, we may construct a plot of $(ft)^{-1}$ versus $|M_{GT}|^2$, which Eq. (25) implies will be a straight line with intercept g_F^2 and slope g_{GT}^2.

Using the $|M_{GT}|^2$ deduced by Trigg[27] for LS coupling and the ft values from Table III, we obtain Fig. 25. The departures from a straight line are no less extensive for jj coupling, in particular $|M_{GT}|^2 = 3$, for P^{29} and S^{31} in both couplings.[76]

Jensen and Mayer[26] have noted that the daughter nuclei of both these isotopes have magnetic moments that deviate considerably from those predicted by strict jj coupling symmetry, i.e., the Schmidt model. They have gone on to show that for mirror nuclei there exists a definite relationship between $|M_{GT}|^2$ and the nuclear magnetic moment,

$$|M_{GT}|^2 = \frac{J+1}{J}\left|\frac{2\mu - \frac{J}{j}(\ell + 0.88)}{4.70 + \ell}\right|^2 : j = \ell + 1/2, \qquad (26\,a)$$

$$|M_{GT}|^2 = \frac{J+1}{J}\left|\frac{2\mu - \frac{J}{j+1}(\ell + 0.12)}{3.70 - \ell}\right|^2 : j = \ell - 1/2, \qquad (26\,b)$$

if the assumptions are made that jj coupling is in operation for charge-independent nuclear forces.

The validity of these formulae rests on the fact that the theoretical values for both M_{GT}^2 and the magnetic moment depends on the evaluation of the same expectation value,[78]

$$\left\langle \sum_i \sigma_0^{(i)} t_Z^{(i)} \right\rangle .$$

Thus we have essentially evaluated this integral with the experimental magnetic moment and then substituted into the formulae for M_{GT}^2.

Using these formulae we have computed $|M_{GT}|^2$ from the experimental magnetic moments and compared them with the experimental

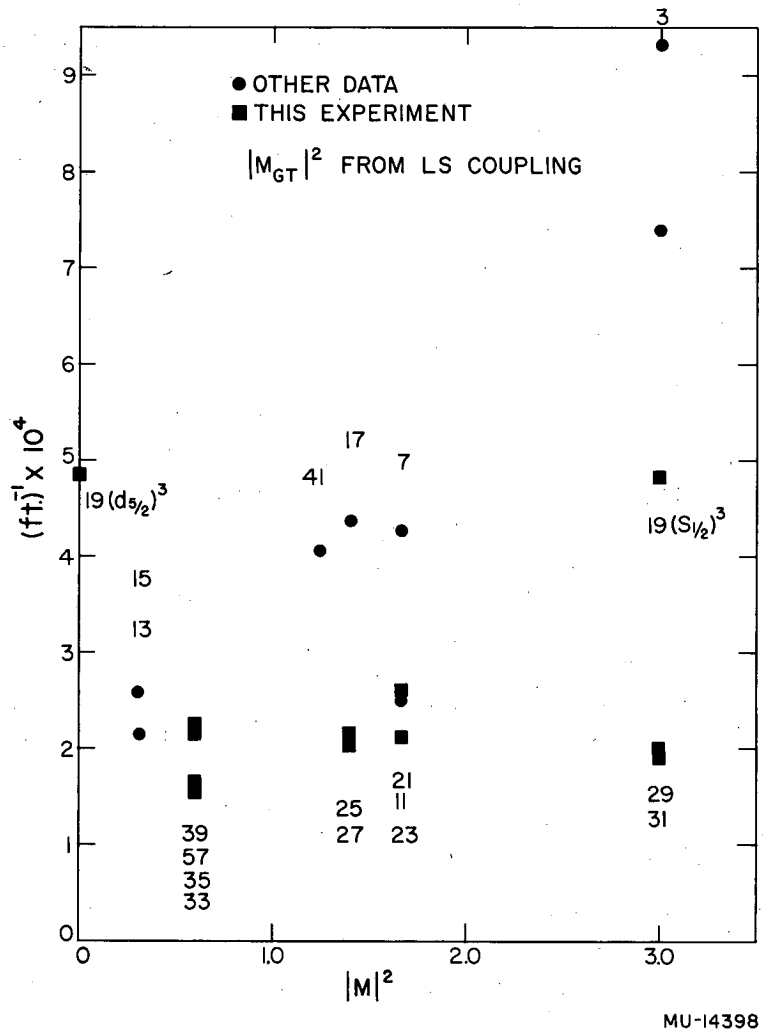

Fig. 25. Experimental values of $(ft)^{-1}$ versus values of the Gamow-Teller matrix element computed on the basis of LS coupling. Because the Fermi matrix element is almost certainly equal to one, the plot should be a straight line. Matrix elements from jj coupling fit no better. Compare with Fig. 26.

ft values by means of Eq. (25) in Fig. 26. The fit is relatively good and some of the deviation may be removed by the proper inclusion of branching-ratio corrections (see Section III-D). This analysis gives the values

$$g_F^2 = 1.5 \cdot 10^{-4} \text{ sec}^{-1}, \tag{27a}$$

$$g_{GT}^2 = 2.1 \cdot 10^{-4} \text{ sec}^{-1}; \tag{27b}$$

the former is in excellent agreement with that deduced by Gerhart[79] from the decay $O^{14} \rightarrow N^{14*}$. An equally good fit to the same values of g (with the exception of the point for He^3) can be obtained from semi-empirical matrix elements of Trigg,[27] who adjusted his LS matrix elements according to deviations of the experimental magnetic moment from corresponding computed values.

The value of the ratio g^2_F/g^2_{GT} is in good agreement with those obtained by Gerhart,[79]

$$g^2_F/g^2_{GT} = 0.56 \text{ to } 0.93;$$

Blatt,[80]

$$g^2_F/g^2_{GT} = 0.29 \text{ to } 1.04;$$

and Kofoed-Hansen,[81]

$$g^2_F/g^2_{GT} = 0.82 \text{ to } 1.22.$$

The first two analyses are based on data from O^{14}, H^3, N^1, and He^6. The last one was based on N^1, H^3, O^{15}, F^{17}, Ca^{39}, and Sc^{41}. Kofoed-Hansen also noted that the other mirror data could be put into a pattern only by using matrix elements adjusted to magnetic moments.

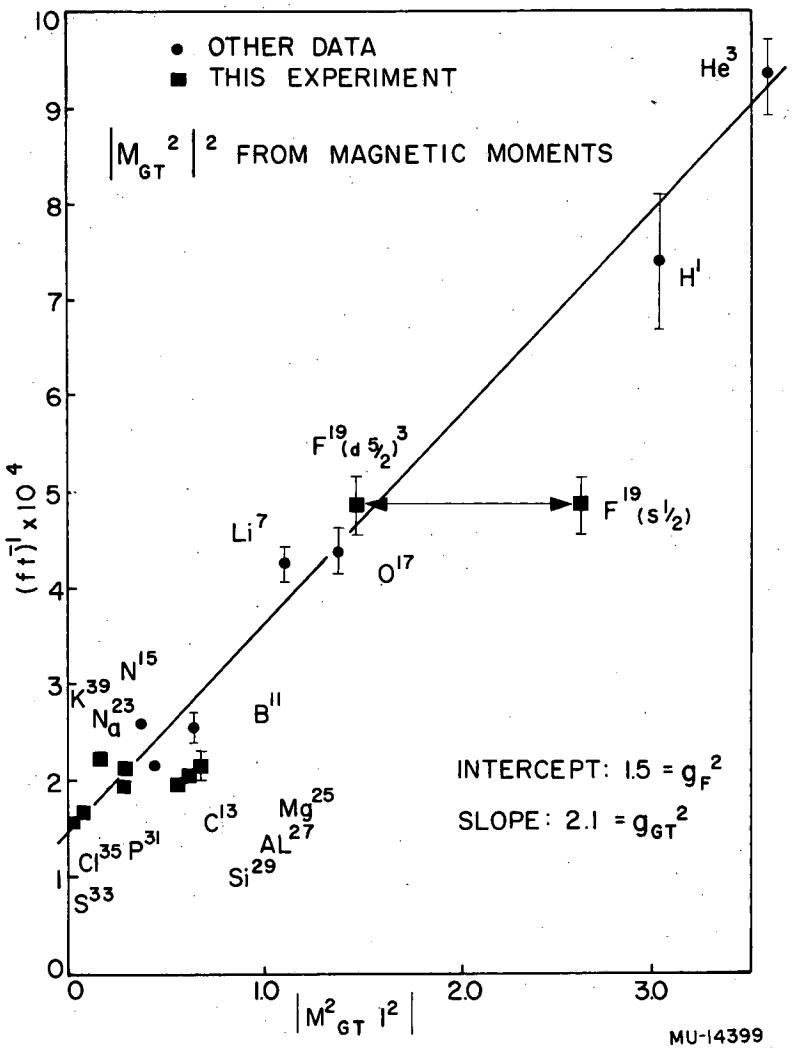

Fig. 26. Experimental values of $(ft)^{-1}$ versus values of the Gamow-Teller matrix element calculated from experimental nuclear magnetic moments for jj coupling.[26] Because the Fermi matrix element is almost surely equal to 1, the plot yields g_F^2 and g_{GT}^2 for intercept and slope respectively. The fit to a straight line is noticeably better than Fig. 25. Matrix elements for LS coupling adjusted for experimental magnetic moments[27] fit almost as well to the same values of g^2.

V. CONCLUSIONS

The data for this experiment show clearly that an even-odd alternation (even Z → odd Z versus odd Z → even Z) of the Coulomb energy differences between mirror nuclei extends to A = 41. It further shows modifications of the basic alternation, just as would be predicted by a shell model with strong spin-orbit coupling. The observed energy differences can be explained in detail by the symmetry properties of shell model, using harmonic oscillator wave functions and jj coupling in the state of lowest seniority. Nuclear radii calculated on the basis of this model form a consistent picture. They agree with radii measured by high-energy electron scattering and μ-meson x-rays except in the region around A = 24. Here it is proposed that nuclear deformation effects render radii predicted from the model invalid. Values of ft from this experiment, when combined with nuclear matrix elements deduced from experimental magnetic moments, form a coherent set of data. They give values of the β-decay interaction constant for both the Fermi and Gamow-Teller interactions.

ACKNOWLEDGMENTS

The author is indebted to and wishes to express his gratitude to the people who have helped make this paper possible:

Professor Luis W. Alvarez, who suggested the experiment and who supervised and encouraged the research;

Robert Layman, who built much of the special equipment and who contributed many long hours and hard work during the setting up and execution of the experimental runs and data reduction; James Sirois and the linear accelerator crew, not only for operation of the accelerator, but also for their help in fabricating and repairing some of the equipment; Barkley Jones and the 60-inch cyclotron crew, for modifications of the cyclotron operation which they made to accommodate this experiment;

Dr. Roger Wallace, for the design and construction of the spectrometer and his help and advice throughout the experiment; Don Gow, for his assistance during the early runs and his continued interest in the experiment; Wade Patterson and Bob Cence, for early work in setting up the spectrometer; Dr. John Brabant and Dr. Selig Kaplan for design and construction of the tandem gate apparatus; Dr. John Wiggin for assistance during the closing runs;

Dr. Warren Heckrotte and Jack Uretsky, for their helpful discussion concerning the theory;

Dr. John S. Foster, UCRL Livermore, and Col. Edward Giller, USAF, for their cooperation in enabling the author to perform this experiment;

Dr. Wilmot Hess and many other friends and colleagues whose interest, advice, and encouragement have been invaluable; and

Carroll Wright Welch, the author's wife, for her sustaining encouragement and excellent assistance with the calculations, plotting, and typing.

This work was done under the auspices of the U. S. Atomic Energy Commission.

REFERENCES

1. E. Feenberg and G. Goertzel, Phys. Rev. 70, 597 (1946).
2. D. R. Inglis, Revs. Modern Phys. 25, 39 (1953).
3. M. Mayer and J. Jensen, Elementary Theory of Nuclear Shell Structure, (Wiley, New York, 1955) p. 27
4. H. A. Bethe and R. F. Bacher, Revs. Modern Phys. 8, 82 (1936).
5. C. F. von Weizsäcker, Z. Physik 96, 431 (1935).
6. L. N. Cooper and E. M. Henly, Phys. Rev. 92, 801 (1953).
7. R. R. Wilson, Phys. Rev. 88, 350 (1952).
8. J. B. Ehrmann, Phys. Rev. 81, 412 (1951).
9. B. G. Jancovici, Phys. Rev. 95, 389 (1954).
10. B. C. Carlson and I. Talmi, Phys. Rev. 96, 436 (1954).
11. O. Kofoed-Hansen and Aage Winther, Phys. Rev. 86, 428 (1952).
12. D. C. Peaslee, Phys. Rev. 95, 717 (1954).
13. Kistner, Schwarzchild, and Rustad, Bull. Am. Phys. Soc. I 1, 30 (1956).
14. C. R. Sun and B. T. Wright, Bull. Am. Phys. Soc. II 1, 253 (1957).
15. Roderick, Lönsjö, and Meyerhof, Phys. Rev. 97, 97 (1955).
16. Kistner, Schwarzchild, and Rustad, Phys. Rev. 104, 154 (1956).
17. R. W. King, Revs. Modern Phys. 26, 327 (1954).
18. D. R. Eliot and L. P. D. King, Phys. Rev. 60, 489 (1941).
19. D. M. Endt and J. C. Kluyver, Revs. Modern Phys. 26, 95 (1954).
20. N. W. Glass and J. R. Richardson, Phys. Rev. 98, 1251 (1955).
21. D. H. Wilkinson, Phil. Mag., Series 8, 1, 1031 (1956).
22. K. W. Ford and D. L. Hill, Annual Review of Nuclear Science, Vol. 5 (Annual Reviews, Stanford, 1955), p. 25.
23. R. Hofstader, Revs. Modern Phys. 28, 214 (1956).
24. J. M. C. Scott, Progr. in Nuclear Phys. 5, 157 (1956).
25. E. Feenberg and G. Trigg, Revs. Modern Phys. 22, 399 (1950).
26. Mayer and Jensen, op. cit. p. 177.
27. G. L. Trigg, Phys. Rev. 86, 506 (1952).
28. Beta and Gamma-Ray Spectroscopy, Kai Siegbahn, Ed. (North Holland, Amsterdam, 1955).

29. E. Persico and C. Geoffrion, Rev. Sci. Instr. 21, 945 (1950).
30. C. Geoffrion, Rev. Sci. Instr. 20, 638 (1949).
31. E. Fermi, Nuclear Physics (Univ. of Chicago Press, 1955), p. 36.
32. National Bureau of Standards, Tables for the Analysis of Beta Spectra (U. S. Govt. Printing Office, 1952), p. 21.
33. G. Schrank and J. R. Richardson, Phys. Rev. 86, 248 (1952).
34. Toppel, Wilkinson, and Alburger, Phys. Rev. 101, 1485 (1956).
35. D. M. Van Patter and W. Whaling, Revs. Modern Phys. 26, 402 (1954).
36. J. C. Hubbs and G. M. Frosof, Phys. Rev. 104, 715 (1956).
37. Joan M. Freeman, Phil. Mag., Ser. 8, 1, 591 (1956).
38. R. L. Seale, Phys. Rev. 92, 389 (1953).
39. W. G. Read and R. W. Krone, Phys. Rev. 104, 1018 (1956).
40. W. W. Buechner and A. Sperduto, Phys. Rev. 106, 1008 (1957).
41. Schiffer, Gossett, Phillips, and Young, Phys. Rev. 103, 134 (1956).
42. White, Delsasso, Fox and Creutz, Phys. Rev. 56, 512 (1939).
43. Ager-Hannssen, Lonsjo, and Nordhagen, Phys. Rev. 101, 1779 (1956).
44. Rayburn, Lafferty and Hahn, Phys. Rev. 98, 701 (1955).
45. Van Patter, Porter, and Rothman, Phys. Rev. 106, 1016 (1957).
46. P. M. Endt and C. H. Paris, Phys. Rev. 106, 764 (1957).
47. Paris, Buechner and Endt, Phys. Rev. 100, 1317 (1955).
48. W. E. Meyerhof and G. Lindstrom, Phys. Rev. 93, 949 (1954).
49. Endt, Paris, Sperduto, and Buechner, Bull. Am. Phys. Soc. II, 2, 178 (1957).
50. J. P. Schiffer, Bull. Am. Phys. Soc. II, 1, 95 (1956).
51. Schwarz, Corbett, and Watson, Phys. Rev. 101, 669 (1956).
52. J. R. Holt and T. N. Marsham, Proc. Phys. Soc. 66A, 258 (1952).
53. C. Wong, Phys. Rev. 95, 761 (1954).
54. I. Talmi and R. Theiberger, Phys. Rev. 103, 718 (1956).
55. Marion, Bonner, and Cook, Phys. Rev. 100, 91 (1955).
56. Sherr, Muenther, and White, Phys. Rev. 75, 282 (1949).
57. F. I. Boley, Iowa State Coll. J. Sci. 27, 129 (1953).
58. Hunt, Kline, and Zaffarano, Bull. Am. Phys. Soc, 29, 4, G1 (1954).

59. D. J. Zaffarano and F. I. Boley, Phys. Rev. 84, 1059 (1951).
60. Hunt, Jones, and Churchill, Proc. Phys. Soc. 67A, 479 (1954).
61. Barkas, Creutz, Delsasso, Sutton, and White, Phys. Rev. 58, 383 (1940).
62. McCreary, Kuerti, and Van Voorhis, Phys. Rev. 57, 351 (1940).
63. M. Nahmais and T. Yuasa, Compt. rend. 236, 2399 (1953).
64. White, Creutz, Delsasso, and Wilson, Phys. Rev. 59, 63 (1941).
65. D. R. Elliott and L. D. P. King, Phys. Rev. 59, 403 (1941).
66. R. Braams and C. L. Smith, Phys. Rev. 90, 995 (1953).
67. Paris, van der Leun, and Endt, Bull. Am. Phys. Soc. II 2, 179 (1957).
68. C. M. Braams, Phys. Rev. 94, 763 (1954).
69. H. S. Plendl and F. E. Steigert, Phys. Rev. 98, 1583 (1955).
70. Rubin, Johnson, and Reynolds, Phys. Rev. 104, 1444 (1956).
71. J. M. Blatt and V. F. Weisskopf, Theoretical Nuclear Physics (Wiley, New York, 1953).
72. Richard H. Helm, Phys. Rev. 104, 1466 (1956).
73. Litherland, Paul, Bartholomew, and Gove, Phys. Rev. 102, 208 (1956).
74. Mayer and Jensen, op. cit. p. 158.
75. J. Schwinger, Phys. Rev. 78, 135 (1950).
76. Mayer and Jensen, op. cit., p. 174.
77. I. Talmi, Phys. Rev. 91, 122 (1953).
78. Mayer and Jensen, op. cit., p. 251.
79. J. R. Gerhart, Phys. Rev. 95, 288 (1954).
80. John M. Blatt, Phys. Rev. 89, 83 (1953).
81. Aage Winther and O. Kofoed-Hansen, Kgl. Danske Videnskab. Selskib, Mat-Fys. Medd. 27, No. 14 (1953).